Structural evidence that the polymerization rate dictates order and intrinsic strain generation in photocured methacrylate biomedical polymers

Sirovica, Slobodan; Skoda, Maximilian W. A.; Podgorski, Maciej; Thompson, Paul B. J.; Palin, William M.; Guo, Yilan; Smith, Andrew J.; Dewan, Karun; Addison, Owen; Martin, Richard A.

DOI:
10.1021/acs.macromol.9b00133

Structural evidence that polymerisation rate dictates order and intrinsic strain generation in photo-cured methacrylate biomedical polymers

Slobodan Sirovica[a], Maximilian W.A. Skoda[b], Maciej Podgorski[c,d], Paul B.J. Thompson[e], William M. Palin[f], Yilan Guo[g], Andrew J. Smith[h], Karun Dewan[f], Owen Addison[f,g*] and Richard A. Martin[a*]

[a] Aston Institute of Materials Research, School of Engineering & Applied Science, University of Aston, Birmingham, B4 7ET, UK.

[b] ISIS Pulsed Neutron and Muon Source, Science and Technology Facilities Council, Rutherford Appleton Laboratory, Harwell Science and Innovation Campus, Didcot, OX11 0QX, UK.

[c] Department of Chemical and Biological Engineering, University of Colorado Boulder, 596 UCB, Boulder, CO 80309, USA.

[d] Faculty of Chemistry, Department of Polymer Chemistry, Maria Curie-Sklodowska University, Gliniana Street 33, 20-614 Lublin, Poland.

[e] XMaS The UK CRG, ESRF-The European Synchrotron, Grenoble, France.

[f] College of Medical and Dental Sciences, Institute of Clinical Sciences, School of Dentistry, University of Birmingham, Mill Pool Way, Edgbaston, Birmingham, B5 7EG, UK.

[g] Faculty of Medicine and Dentistry, University of Alberta, Edmonton, T6G 1C9, Canada.

[h] Diamond Light Source Ltd., Diamond House, Harwell Science and Innovation Campus, Didcot, Oxfordshire OX11 0DE, U.K.

*Co-last author and Corresponding author(s)

Corresponding author(s): Owen Addison,
Faculty of Medicine and Dentistry,
University of Alberta,
Edmonton,
Canada.

Telephone: +1 780 492 5308
E-Mail: oaddison@ualberta.ca

Richard Martin,
School of Engineering & Applied Science and Aston Institute of Materials Research,
University of Aston,
Birmingham,
United Kingdom.

Telephone: +44 (0)121 204 5111
E-Mail: r.a.martin@aston.ac.uk

Table of Contents Graphic

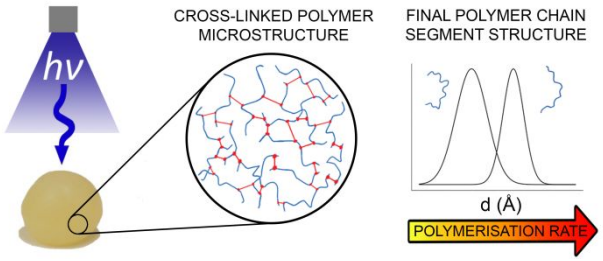

ABSTRACT

The influence of reaction rate on the evolving polymer structure of photo-activated dimethacrylate biomedical resins was investigated using neutron and *in-situ* synchrotron X-ray scattering with simultaneous FT-NIR spectroscopy. Previous studies have correlated the degree of reactive group conversion with mechanical properties, but the impact of polymerisation rate on the resultant polymer structure is unknown. Here we demonstrate that medium-range structural order at the functional end groups of these materials is dependent on reaction rate. Accelerating polymerisation, increases correlation lengths in the methacrylate end groups but reduces medium-range structural order per converted vinyl bond when compared with more slowly polymerised systems. At fast rates of polymerisation, the conformation of atoms at the reacting end group can become fixed into the polymer structure at the onset of auto-deceleration, storing residual strain. Neutron scattering confirms that the structural differences observed are reproduced at longer length scales. This effect is not as prominent in systems polymerised at slower rates despite similar final degrees of reactive group conversion. Results suggest that current interpretations of these materials which extrapolate mechanical properties from conversion may be incomplete. Accelerating polymerisation can introduce structural differences which will dictate residual strain and may ultimately explain the discrepancies in the predictive modelling of the mechanical behaviour of these materials using conventional techniques.

1. INTRODUCTION

Photo-initiated methacrylate polymers are of great biomedical importance as they provide, when compared with chemically-cured alternatives, extended working times for the operator to place and manipulate the material and more rapid setting times once the correct material positioning has been achieved. Photo-initiated methacrylate polymer based materials are routinely used in orthopaedic surgery and in particular in dentistry where they are combined with inorganic filler particles to form resin based-composites. The physiochemical properties of these materials are highly sensitive to photo-polymerisation variables which impact on the degree of reactive group conversion and the development of transient and residual stresses which ultimately affect clinical performance [1–3]. The degree of reactive group conversion is typically measured using Fourier transform infrared (FTIR) or Raman spectroscopy but fails to provide insight into the architecture of the cross-linked polymer structure and the development of strains. This work explores for the first time the effects of polymerisation rate on the development of the medium range (~ 4-15 Å) polymer structure of the most commonly encountered photo-initiated biomedical resin polymers based on methacrylate chemistry, which are used ubiquitously in contemporary dental care.

The majority of contemporary dental resin-composite filling materials are comprised of a dimethacrylate polymer matrix composed of a viscous monomer and reactive low molecular weight diluent monomer(s), combined with nano and/or micron scale inorganic filler particles. Following application to the tooth surface the composite is 'demand-set' by light excitation of a photo-initiator species dispersed within the resin matrix, initiating free radical polymerisation and generating a solid three-dimensional cross-linked polymer network (4, 5). These matrices typically achieve up to ~ 80% conversion of the starting reagents to a polymer structure [6,7]. A higher degree of conversion (*DC*) has been shown to significantly influence resultant mechanical properties, conferring an increased flexural strength, surface hardness [8], elastic modulus and wear resistance [9]. It has therefore been proposed that the final mechanical properties of the composite are determined by the maximum degree of conversion (DC_{max}) which itself can be manipulated by altering the intensity of, and exposure to, the activating light source [10–12]. It has been suggested that DC_{max} is proportional to the total photon

delivery irrespective of how they are delivered, a concept known as exposure reciprocity [13,14]. However, theoretical and experimental approaches have shown that reactions that do not have a first order dependency on the impinging light intensity, such as free radical photo-polymerisation and associated bimolecular processes, do not and should not obey the concept of reciprocity [15]. Monomer structure [16,17], viscosity, co-monomer concentration [18–20] and differences in quantum efficiency [21] and absorption spectra [22,23] of photo-initiator species will all impact on the mobility, polymerisation rate and DC_{max} of these systems. Photo-activated resin composites therefore represent a complex system and an understanding of polymerisation cannot be obtained solely from the measurement of DC_{max}.

Several groups have instead varied the reaction rate and demonstrated a parabolic relationship between the polymerisation rate, DC and the final mechanical properties [24] including tensile strength, toughness, hardness and the magnitude of volumetric shrinkage of the polymer on polymerisation [3,25–27]. To date, these differences in mechanical properties, for similarly converted resin matrices polymerised at different rates, have been ascribed to the cross-link density and its effect on network architecture. Accelerating polymerisation reduces the lifetime of radical species with respect to bimolecular termination [27], limiting the degree of cross-linkage and lowering the strength of the resultant matrix.

Accordingly, efforts have been made to optimise the resin matrix and photo-initiator system composition in terms of polymerisation rate and DC_{max}. However, no consideration has been given as to what effect reaction rate and conversion have on the final polymer structure at short to medium range length scales. Ordering in amorphous materials is typically classified within two length scale regimes; short and medium. Short range order refers to bonding between atoms at length scales between ~ 0-4 Å[28], such as covalent and hydrogen bonds. Medium range ordering describes the interconnection of constituent units within a structure (~ 5-20 Å)[28], which for densely cross-linked dimethacrylate networks includes polymer segments and cross-linking distances. The concept that an identically composed and converted material can demonstrate different structures as a consequence of polymerisation rate arises from consideration of the reaction itself. At increased rates of reactive group conversion and cross-linking, the emerging structure has less time to achieve its most

energetically favourable form. In contrast, slowing the reaction rate may allow the propagating polymer chains to move relatively to find a more energetically efficient state. A difference in structural order (conformation) is therefore hypothesized to exist and such differences may influence the mechanical properties of the material. The challenge in identifying such differences exists because the likely structural differences will occur mainly at short-medium length scales. Scattering measurements using laboratory X-ray sources fail to provide sufficient flux to discern such differences in these materials, especially when dynamic (*in-situ*) curing studies with short measurement times are conducted.

This novel enquiry reports the determination of the cross-linked polymer structure and potential generation of strains within common biomedical photo-activated resin matrices as a function of polymerisation rate through a comprehensive series of synchrotron X-ray scattering, neutron scattering combined with isotopic substitution and complementary FTIR spectroscopic measurements. As there is no previous enquiry in this area the null hypothesis that no relationship between polymerisation rate and structural conformation of the resultant polymer network normalised to *DC* was tested.

2. MATERIALS AND METHODS

2.1. Preparation of photo-polymerisable dimethacrylate resin blends

Two dimethacrylate monomers, bisphenol-A-glycidyl-methacrylate (Bis-GMA and triethyleneglycol-dimethacrylate (TEGDMA) (Sigma-Aldrich, Dorset, UK) were proportioned in 70/30, 60/40, 50/50 and 40/60 (Bis-GMA/TEGDMA) weight percentage (wt. %) ratios and combined to produce mixes. The viscosity of the blend increases with the proportion of Bis-GMA[29]. The monomer blends were combined with a photo-initiator as either 0.2 wt% Camphorquinone (CQ) with 0.8 wt% of its tertiary amine N,N-dimethylaminoethyl-methacrylate (DMAEMA) or 1 wt% of the Type 1 photo-initiator, Lucirin-TPO (TPO) (Sigma-Aldrich, Dorset, UK), which does not require a co-initiator. The proportioned monomers and photo-initiators were homogenised in a glass beaker using a magnetic

stirrer at 50 ± 1 °C for 30 mins in dark conditions. The resultant resin blends were stored in dark conditions in sealed containers at 4 ± 1 °C prior to further use.

2.2. Preparation of pre-polymerised partially deuterated dimethacrylate resin blends

To characterise structure at cross-linking distances the methacrylate end groups of TEGDMA were isotopically substituted with deuterium. Deuterium has a relatively large coherent neutron scattering cross-section [30] and scatters neutrons more efficiently than its lighter counterpart. Isotopic substitution was undertaken for the TEGDMA monomer only, producing d_{10}-TEGDMA (**Figure 1**). Details regarding the synthesis of d_{10}-TEGDMA are included in the supporting materials and methods.

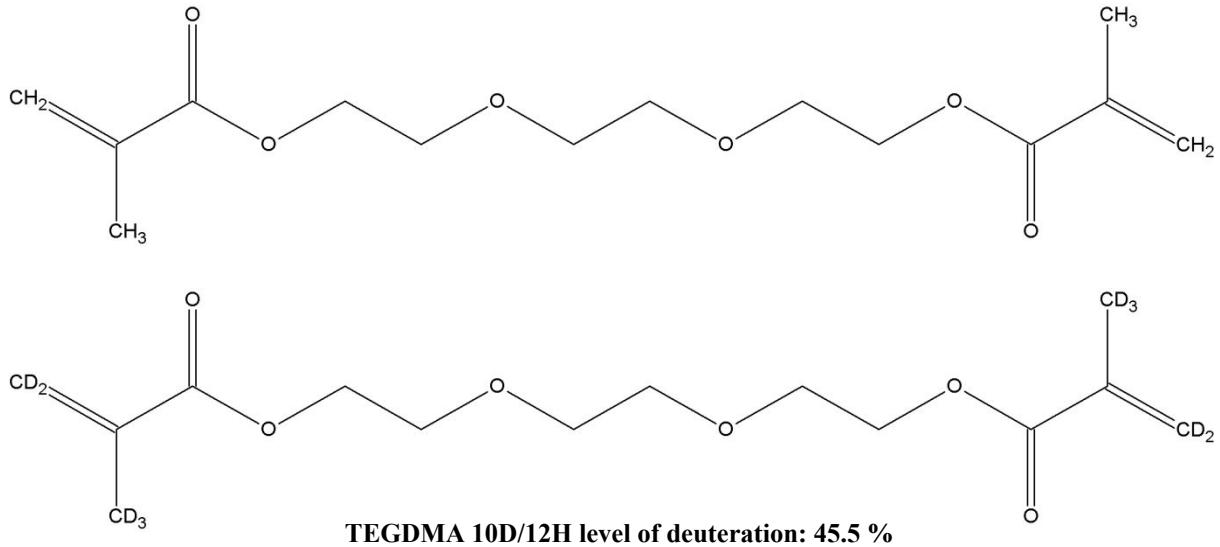

TEGDMA 10D/12H level of deuteration: 45.5 %

Figure 1. (Top) Hydrogenated TEGDMA. **(Bottom)** Partially deuterated TEGDMA monomer with 45.5% deuteration by molecular weight of the original hydrogen atoms.

Partially deuterated resin blends were produced in a similar way to those with a hydrocarbon methacrylate functionality described in 2.1, but with TEGDMA substituted with d_{10}-TEGDMA. As deuterated monomers were produced in significantly smaller quantities only 60/40 and 40/60 wt% blends were prepared.

Resin disc-shaped specimens were fabricated by filling a polyvinylsiloxane mould (11 mm diameter and 1 mm in depth) and then covered with a microscope cover slide to minimise the formation of an oxygen inhibition layer. Specimens were photo-polymerised specimens using an EMS Swiss master light curing unit (EMS OPTIDENT, electro medical systems, Nyon Switzerland) placed normal to and in contact with the cover slide. The curing unit has a spectral output range of 390 – 550 nm to provide significant overlap with the absorption peaks of the Camphorquinone (470 nm) and Lucirin TPO (381 nm) photo-initiators. For each unique composition, the resin was either photo-polymerised at relatively 'high' (3000 mW cm^{-2} for 6 s) or 'low' (300 mW cm^{-2} for 60 s) irradiances ensuring matched total energy doses or radiant exposures (18 J cm^{-2}). The resultant specimens were stored in lightproof conditions in sealed containers at 4 ± 1 °C prior to further use. Samples were purposely manufactured to be no more than 1 mm in thickness to reduce the effects of absorption, incoherent and inelastic scattering which is significant in materials containing hydrogen.

2.3. Simultaneous X-ray scattering and FT-NIR measurements

Simultaneous synchrotron radiation (SR) X-ray scattering/FT-NIR spectroscopy measurements were performed on the I22 beamline (Diamond Light Source, Oxford, UK). An incident X-ray energy of 12 keV was used corresponding to a wavelength of 1.033Å with a beam size of 0.32 × 0.08 mm (horizontal × vertical). Specimens were prepared by filling a 0.9 mm thick stainless steel ring with a 10 mm internal diameter which was sealed on both faces by 25 μm thick mica (Attwater Group, Lancashire, UK). The resin filled rings were housed within a brass block annulus (Daresbury Laboratory, Warrington, UK) and a 5 mm diameter light guide (Lumencor, Kent, UK) was fixed normal to and 15 mm distant from the centre of the resin surface and connected to a multichannel light source (Lumencor Aura Light engine, Lumencor, Kent, UK) and fixed in place to illuminate only the sample that was directly in the path of the X-rays. Samples were mounted to impinge the X-ray beam at a 40° incline in the positive azimuthal direction. For the TPO initiated resins, a filter within the light engine was used to emit a peak emission spectrum at 405 nm, whilst for CQ systems a wavelength of 470 nm was employed. The light filters and their corresponding wavelengths were chosen to achieve the greatest overlap with the maxima in the visible region of the absorption spectra

of the respective photo-initiators [31]. For each unique composition, samples of monomer blends (n=3, per composition) were photo-polymerised at four different irradiances for each wavelength controlled by the power output of the light engine (5, 20, 60 and 100% power output) for a total of 300 s. Irradiances were calculated by spectrometry measurements for each testing set-up, light source and power setting and are reported with the experimentally related scattering data. 2D scattering patterns were collected every second (1 s readout) throughout polymerisation with a Pilatus (P3-2M) detector providing a q range of 0.1 to 1.6 $Å^{-1}$, where $q = 4\pi/\lambda \sin\theta$. Additional measurements were made using a 400 μs time resolution to confirm that a one second capture rate, used for all other scattering measurements, accurately characterised dynamic structural changes.

X-ray measurements were acquired for the constituent monomers (Bis-GMA and TEGDMA) in isolation and containing photo-initiator to identify their contributions to the scattering signal of each blend through weighted least squares (WLS) fitting. The contribution of the X-ray beam to the measurements was assessed by conducting observations for over 30 mins for the uncured and polymerised samples in the absence of light. To aid data analysis, measurements were taken for direct beam, empty sample containers, mica windows, water and a silver behenate calibration standard to allow the scattering patterns to be corrected for background and normalisation effects. Transmitted beam was recorded throughout using a beam-stop mounted photodiode. In addition to *in-situ* photo-polymerisation measurements and control/calibration measurements, scattering patterns were obtained for control molecules that possess similar structures to those under investigation (methacrylic acid, methyl methacrylate, ethylene glycol, tri-ethylene glycol, bisphenol A and bisphenol A dimethacrylate (all Sigma-Aldrich, Dorset, UK)). The data were normalised and background corrected using the DAWN software package (version 2.8.0, 2017, Diamond Light Source, Oxford, UK) [32,33]. Data were azimuthally averaged over 360° to produce a 1D output and were subsequently fitted with pseudo-Voigt models to obtain the peak centre and the full width at half maximum (FWHM).

To confirm the observations from the I22 beam line, additional synchrotron X-ray scattering measurements were performed on the XMaS beam line (BM28) at the European Synchrotron

Radiation Facility (ESRF, Grenoble, France). An incident X-ray energy of 15 keV was used corresponding to a wavelength (λ) of 0.82 Å, with a beam size of 0.08 × 0.5 mm (horizontal × vertical). A similar experimental geometry was used to that described in Section 2.3 and additional details for this experiment can be found in the supporting materials and methods.

In-situ real time Fourier transform near infrared (FT-NIR) spectroscopy was incorporated into the beamline set-up to obtain simultaneous (to the scattering data) measurements of reactive group conversion throughout photo-polymerisation to enable $DC_{\max}$ and maximum reaction rate (Rp_{max}) to be calculated. Optical (emitting and receiving) fibres (0.6 mm core diameter) (Helma Analytics, Essex, UK) were placed either side of the sample at a 45° incline relative to the sample face and connected to a Nicolet IS50 spectrometer (Thermo Scientific, Warrington, UK), **Figure 2**. During photo-polymerisation, NIR spectra were collected in transmission mode using a white light source and an InGaAs detector. Real time NIR spectra (4000 to 10000 cm^{-1}) were collected in transmission mode (4 cm^{-1} spectral resolution) for 300 s with an integration time of 0.3 s. Reactive group conversion was determined from the aliphatic C=CH_2 IR absorption band (6164 cm^{-1}), located within the methylene functional end groups of the Bis-GMA and TEGDMA monomers. As polymerisation progressed, this absorption peak decreased as C=C bonds were converted to single C-C. Conversion of the vinyl bonds (DC) is given as a percentage of the initial reagent C=C concentration,

$$DC = \left(1 - \left(\frac{=CH_2^{polymer}}{=CH_2^{monomer}}\right)\right) \times 100 \qquad (1)$$

where $=CH_2\ ^{monomer}$ refers to the integrated peak intensity of the band prior to polymerisation (in the monomer state) whilst $=CH_2\ ^{polymer}$ corresponds to the integrated peak intensity for the i^{th} measurement. The rate of polymerisation was calculated as the first derivative of DC with respect to time. Additional spectral profiles were taken of the empty cell, mica windows and of the monomer to correct for background subtraction and intensity normalisation. Data were baseline corrected using Omnic software (Omnic Specta software, version 8.0, Thermo Fisher Scientific, Oxford, UK).

Separate laboratory FT-NIR spectroscopy measurements, replicating the sample geometry and irradiance regimen described in section 2.3, were performed to confirm the observations of *in-situ* observations (see supporting materials and methods).

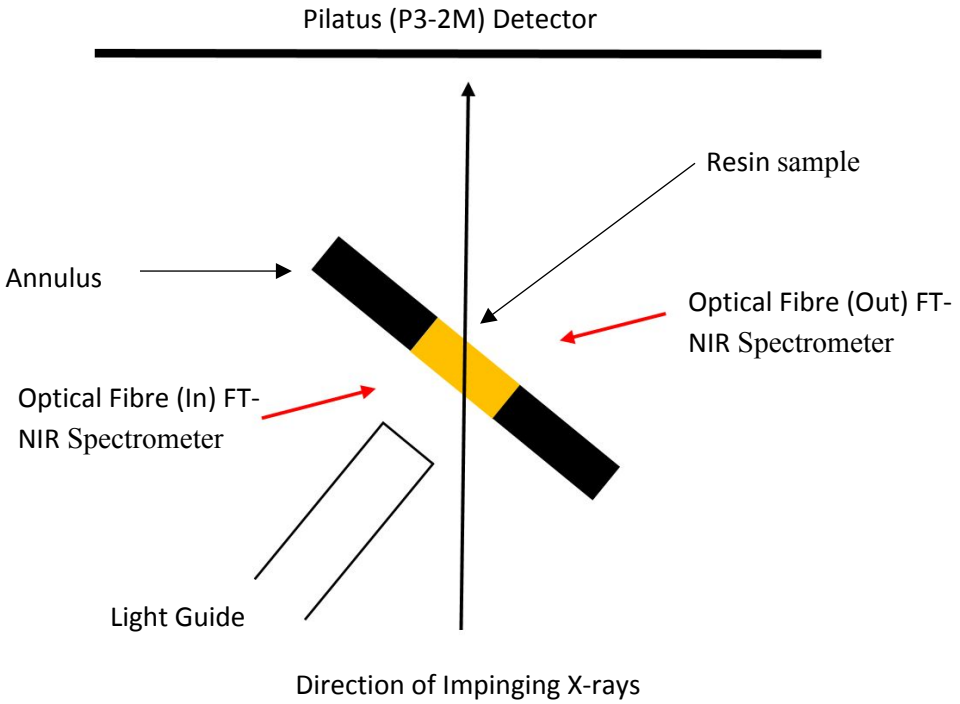

Figure 2. Experimental setup for simultaneous synchrotron SAXS and real time FT-NIR spectroscopy measurements. The resin samples were cured for 300 s at varying light intensities whilst undertaking SAXS and FT-NIRS to quantify changes in the evolving polymer structure and the degree of reactive group conversion respectively.

2.4. Small angle neutron scattering

Small angle neutron scattering (SANS) measurements were performed on the SANS2D[34] instrument at the ISIS pulsed neutron source (Rutherford Appleton Laboratories, Oxford, UK). Disc-shaped resin samples were sealed within aluminium foil and mounted on a cadmium sample rack. SANS2D is a time of flight (TOF) instrument which uses a wavelength range of 1-12 Å to provide a q range of 0.004 – 2 $Å^{-1}$. An 8 mm (diameter) beam size was used to collect SANS data in a transmission mode geometry using a 2D area detector (Ordela, $^3He - CF_4$, Oak Ridge National Laboratory, Tennessee, USA) [35]. Acquisition times per sample were approximately 1 hr and additional measurements were also taken on hydrogenated sample counterparts to serve as controls. Further measurements were

taken for the direct beam, empty sample rack, sample transmission, aluminium foil and a vanadium calibration standard to correct for background and transmission effects and to normalise the data to absolute scattering units respectively. Data were reduced to 1D in absolute scattering units using the SANS2D plugin for the Mantidplot [36] software package (version 3.8.0, 2016, Oxford, UK).

2.5. Thermal changes during photo-polymerisation

Thermal variations associated with photo-polymerisation were characterised and correlated with X-ray scattering data. Temperature measurements were performed at a frequency of 10 Hz using Type K thermocouples with a 0.2 mm tip and a Pico TC-08 data logger (Pico Technology, UK). Ring moulds equivalent to those used for X-ray scattering measurements were filled with a 60/40 wt% Bis-GMA/TEGDMA monomer blend with either a CQ or TPO photo-initiator. The monomer blends were photo-polymerized at an irradiance of ~730 mW cm^{-2} using a Bluephase® Style 20i LED curing light (Ivoclar Vivadent, Schaan, Liechtenstein) for 180 s. For each photo-initiator system, three measurements were conducted with the thermocouple tip placed centrally within the resin and an additional three with the tip at the sample surface. For each thermocouple position, corresponding measurements on an empty mould; a mould containing monomer with no photo-initiator and a mould containing the polymerized polymer were taken for 180 s to allow heating attributable to the curing light to also be estimated.

2.6. Simultaneous X-ray scattering and heating measurements

To correlate temperature with changes in the polymer structure, synchrotron X-ray scattering experiments were performed on the I16 beamline at the Diamond Light Source (Oxford, UK).[37] An incident X-ray energy of 12 keV was used corresponding to a wavelength (λ) of 1.033 Å, with a beam size of 30 μm (vertical) × 200 (horizontal) defined by vacuum tube slits. Measurements were carried out in air with light excluded.

A bespoke heating module was used to increase the temperature of a pre-polymerised 60/40 wt% Bis-GMA/TEGDMA resin disc specimen (10 mm diameter and 0.9 mm thickness) produced according to

the previously described methods, whilst undertaking simultaneous X-ray scattering measurements. The heating module consisted of an aluminium plate (25 × 25 mm area) with a 3 mm (diameter) circular aperture, to allow for the transmission of X-rays, fixed in contact perpendicular to a kinematic heating platform. The temperature of the heating platform was remotely controlled via a cryogenic temperature modulator (model 3.8, Lake Shore cryotonics, Elliot Scientific Ltd, Hertfordshire, UK). Polymer disc specimens were held in tight contact between two aluminium plates. The temperature of test specimen was increased through heat transfer from the kinematic stage to the aluminium plates and finally to the resin disc. Three thermocouples were placed in contact with the kinematic stage, aluminium plates and the resin disc respectively to measure the temperature of each component. The heating module and housed sample were orientated with the annulus of the aluminium plate normal to the path of the impinging X-rays.

X-ray scattering measurements were taken at 5°C increments, from 20 to 60°C, to characterise structural changes as a function of temperature. X-ray scattering data was collected using a 2D area detector (Pilatus 100K) with a 487 x 195 pixel format (pixel size = 172 × 172 μm^2) fixed on to a two theta detector arm. The detector was placed 470 mm behind the sample and collected scattering data at angles of 2θ =7, 13 and 22 to cover a q range of 0.2 to 1.8 $Å^{-1}$ where $q = 4\pi\sin\theta/\lambda$ for each 5°C temperature increment. Scattering data were collected with a 1 s count time and a 2.7 ms readout time. Transmitted beam was also recorded at each angle and temperature increment using a photodiode to correct for changes to the sample density and thickness. To aid data analysis measurements were taken for direct beam, empty sample containers, and a silver behenate calibration standard. Scattering patterns were background corrected and normalised to the incident monitor intensity. Data were azimuthally integrated over 360° to produce a 1D output and were subsequently fit with a pseudo-Voigt model to determine peak positions of correlation lengths as a function of temperature.

2.7. Statistical Analysis

A one tailed paired Students t-test was used to determine differences in the change in correlation length (α=0.05) where factors were photo-initiator chemistry, irradiance protocol and relative

differences in resin matrix viscosity. Statistical analysis was performed in the R programming (version 3.1.3, 2015, R Foundation).

3. RESULTS

3.1. De-convolving the contributions of monomeric components to the scattering signal

Figure 3(a) shows the radially averaged X-ray scattering profile for a TPO initiated 60/40 wt% Bis-GMA/TEGDMA resin blend in its monomer form prior to photo-polymerisation (solid black line), and in the polymer state at 6 s of 300 s of constant irradiation at an intensity of 450 mW cm^{-2} (dotted black line). We observed a broad scattering feature, typical in all observed resin blends, with a peak initially located at q ~1.35 ± 0.0024 Å^{-1} corresponding to a correlation length of 4.65 Å in real space, which moved to lower values of q, approximately 1.23 ± 0.0024 Å^{-1} (5.1 Å) and incrementally narrowed throughout photo-polymerisation. The shift to lower q is indicative of a net length increase of segments within the polymer chain, whilst a narrowing of the peak demonstrates an increase in the medium range (<10 Å) relative structural order.

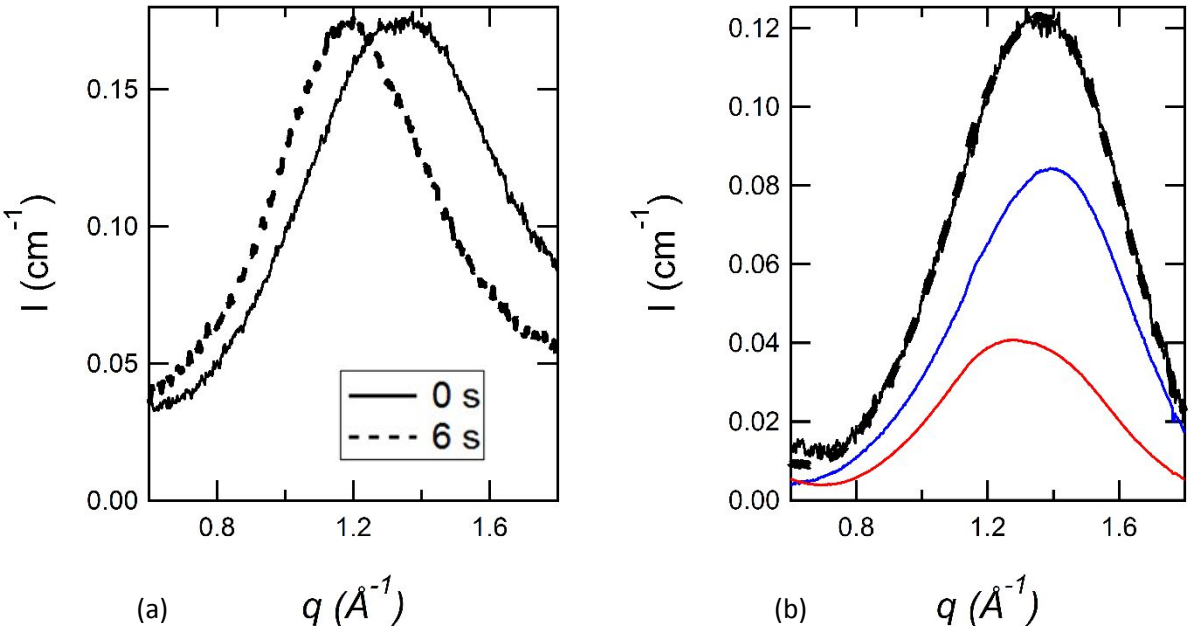

Figure 3. Representative plots showing **(a)** X-ray scattering of a 60/40 Bis-GMA/TEGDMA resin blend initiated with TPO using constant light application at an intensity of 450 mW cm^{-2} for 300 s. Prior to polymerisation (bold black line, at 0 s), a broad Gaussian feature is centred at q ~1.35 Å^{-1} which narrows and moves to q~1.25 Å^{-1} (broken black line, measured at 6 s). **(b)** Weighted least squares fitting (broken black line) of scattering data from the individual Bis-GMA (red) and TEGDMA (blue) monomers to the 60/40 wt% blend (solid black line) following baseline corrections. Bis-GMA and TEGDMA contribute 30 and 70 % to the signal respectively. Data were obtained from I22 (Diamond Light Source).

Figure 3(b) demonstrates the weighted least squares fitting (WLS) of Bis-GMA and TEGDMA X-ray scattering spectra to the signal of the 60/40 wt% resin blend. WLS helped to identify the structural origin responsible for the peak shift with respect to individual monomer contributions to the observed signal. TEGDMA was the predominant contributor to the observed scattering peak (q ~1.35 Å^{-1}) and its shift, accounting for 70 % of the shift whilst only 30 % was attributed to Bis-GMA. The contribution of each monomer to the signal varied with the composition of the resin blend.

Figure 4 illustrates the chemical structures of TEGDMAs' constituent monomers (methacrylic acid and triethylene glycol). **Figure 5** shows the fitting of the TEGDMA X-ray scattering signal based upon the scattering data for the constituent monomers to approximate its chemical structure. WLS fitting reveals that ~68 % of the TEGDMA signal was attributed to methacrylic acid, representing the methacrylic functional end groups (34% per end group) (**Figure 4**). The remaining ~32 % of the TEGDMA signal contribution originated from its ether backbone. Furthermore, ~48 % of the 60/40 wt% Bis-GMA/TEGDMA (total) signal was attributed to methacrylic acid (representing the methacrylate functional end groups) originating from the TEGDMA monomer and ~22 % was weighted to the triethylene glycol component (representing the ether backbone) of the same monomer. Only ~30 % of the change in the scattering peak shift and narrowing following photo-polymerisation of the resin-blend was ascribed to Bis-GMA. For a 60/40 wt% blend the non-aromatic segments of the Bis-GMA monomer contribute ~30% to the total molecular weight of the 60/40 wt% blend. This was equivalent to the contribution that Bis-GMA makes to the scattering signal for the broad feature observed in **Figure 3**.

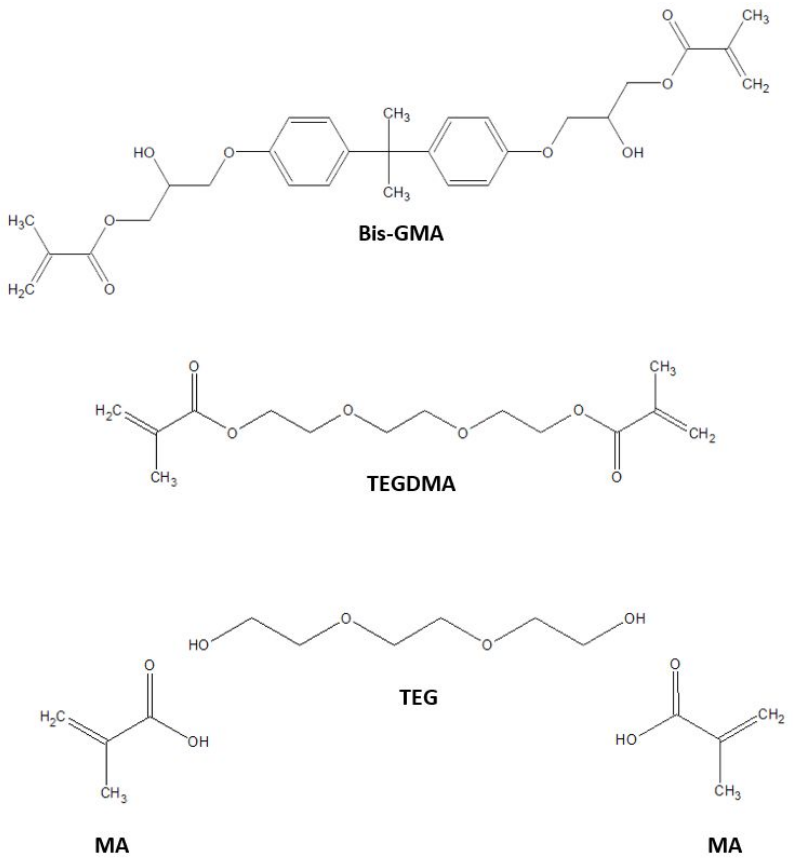

Figure 4. Chemical structures of Bis-GMA and TEGDMA monomers used to formulate each blend. Methacrylic acid (MA) and triethylene glycol (TEG) were used to simulate the chemical structure and dynamic behaviour of the TEGDMA monomer during polymerisation.

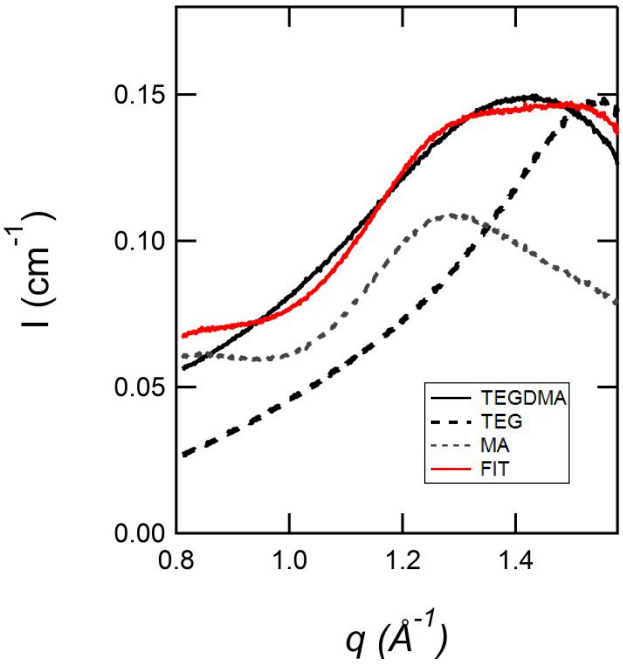

Figure 5. WLS fitting of methyl methacrylate (MA) and triethylene glycol (TEG) X-ray scattering to that of TEGDMA. MA and TEG were used to approximate both the structure and X-ray scattering pattern of the TEGDMA monomer. Close to 70% of the shift and narrowing in scattering following polymerisation was attributed to MA with the remainder ascribed to TEG. Data were obtained from I22 (Diamond Light Source).

Figure 6 shows the 1D neutron scattering spectra for TPO initiated 60/40 wt%.(Bis-GMA/d_{10}-TEGDMA) resin blends, either prior to polymerisation as the liquid monomer (solid black line) or after, when photo-polymerised at either relatively fast (3000 mW cm^{-2}, black dots) or slow (300 mW cm^{-2}, broken black line) rates. It can be seen that a broad scattering peak is initially located at ~ 0.69 $Å^{-1}$ (~9.1 Å), which shifts to lower q and narrows in width following photo-polymerisation, indicative of a net increase in the correlation length and medium range order that this scattering peak represents. Systems polymerised at relatively fast rates demonstrated a greater peak shift to lower q ~ 0.57 $Å^{-1}$ (~11 Å) compared with slower polymerisation where q~0.62 $Å^{-1}$ (~10.1 Å). Similarly, systems polymerised at relatively low and high irradiances displayed FWHM values of ~ 0.13 and 0.15 $Å^{-1}$, where a reduced peak width corresponds to greater structural order. **Figure 6** also displays the neutron scattering spectra of a 60/40 wt% (Bis-GMA/TEGDMA) resin blend (dashed-dotted line) with a hydrocarbon methacrylate functionality which displays no scattering features in the region up to q ~ 1 $Å^{-1}$.

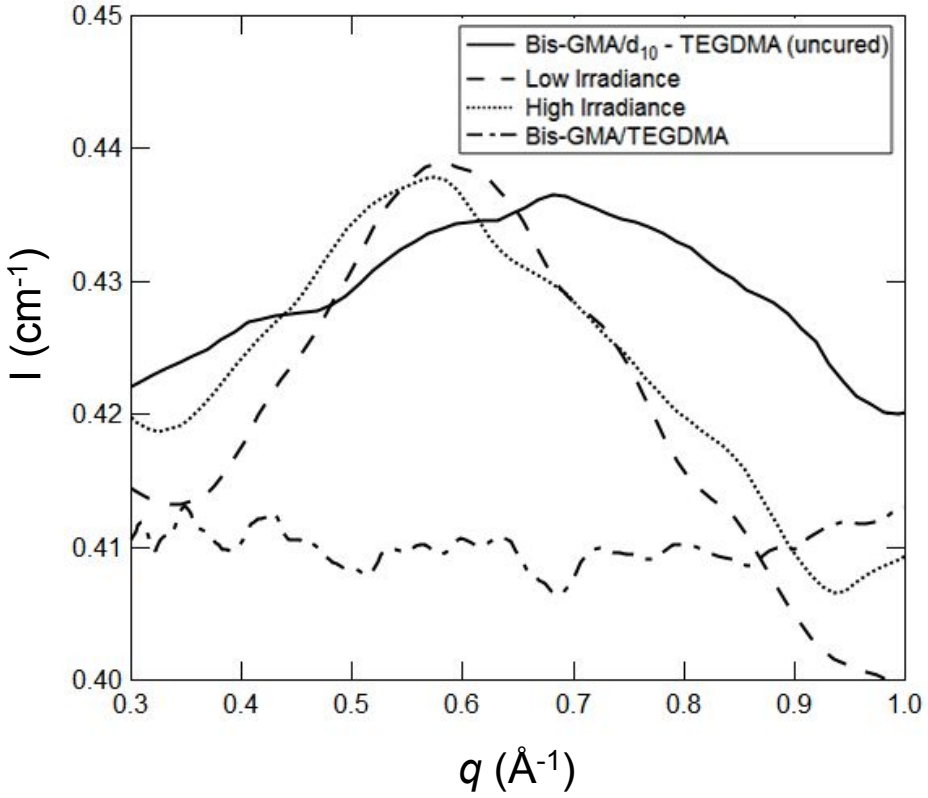

Figure 6. A representative plot of neutron scattering spectra for resins with deuterated or hydrocarbon methacrylate functionality based on a 60/40 wt% blend of Bis-GMA/d_{10}-TEGDMA or Bis-GMA/TEGDMA respectively. A broad scattering peak is observed for the deuterated liquid monomer blend at ~ 0.68 $Å^{-1}$ (-), which shifts to lower q and narrows following photo-polymerisation. Accelerating polymerisation through high light irradiance confers a greater shift to lower q (•••) compared with slower polymerisation (---). Blends with a hydrocarbon methacrylate functionality display no structural features within this q range (- • -).

3.2. The effect of polymerisation rate on the evolving polymer structure

Figure 7 illustrates the real time behaviour of the correlation length and increase in the relative structural order for a 50/50 wt% resin blends. The correlation length corresponds to the average bond length as taken from the peak position in **Figure 3 (a)**, whilst the relative structural order refers to the distribution of correlation lengths calculated from the full width half maximum of the same scattering peak. This formulation displays typical structural changes observed in all of the resin blends for varying viscosities at relatively fast and slow polymerisation rates (controlled by light intensity and photo-initiator chemistry). The peak position of the broad scattering feature observed in **Figure 3(a)** is shown in real space (Å) for each time point (every second) during light irradiation, representing an increase in the correlation length (**Figure 7a** and **b**).

Resins polymerised at faster and slower reaction rates both displayed an increase in the correlation length. For slower polymerisation, typically initiated with CQ for all light intensities, this increase occurs in two stages; a relatively large and fast increase to a local maxima followed by a gradual gain with time (**Figure 7a**, red line). Increasing the polymerisation rate (initiating with TPO and photo-curing with higher irradiance) conferred a significantly greater increase in the correlation length ($p < 0.01$) in a shorter period of time, with the magnitude of this initial extension more than double that observed at the lowest polymerisation rate (**Figure 7a**). An additional decrease in length is also observed following initial extension for faster polymerisation and is equal to approximately 5-15% of the initial extension, depending on the intensity of the activating light (see supporting data for additional results). A small subsequent increase was observed in the correlation length for most blends transitioning either directly from the initial extension or from this relaxation, depending on the polymerisation rate. It can be seen that the final (observed) correlation length remained smaller for more slowly polymerised resins. The magnitude of the gradual extension phase is less for faster polymerisation and always followed relaxation. The slow increase in the correlation length was larger when the system was polymerised with a lower light irradiance, whereas resins polymerised more rapidly show little or no increase.

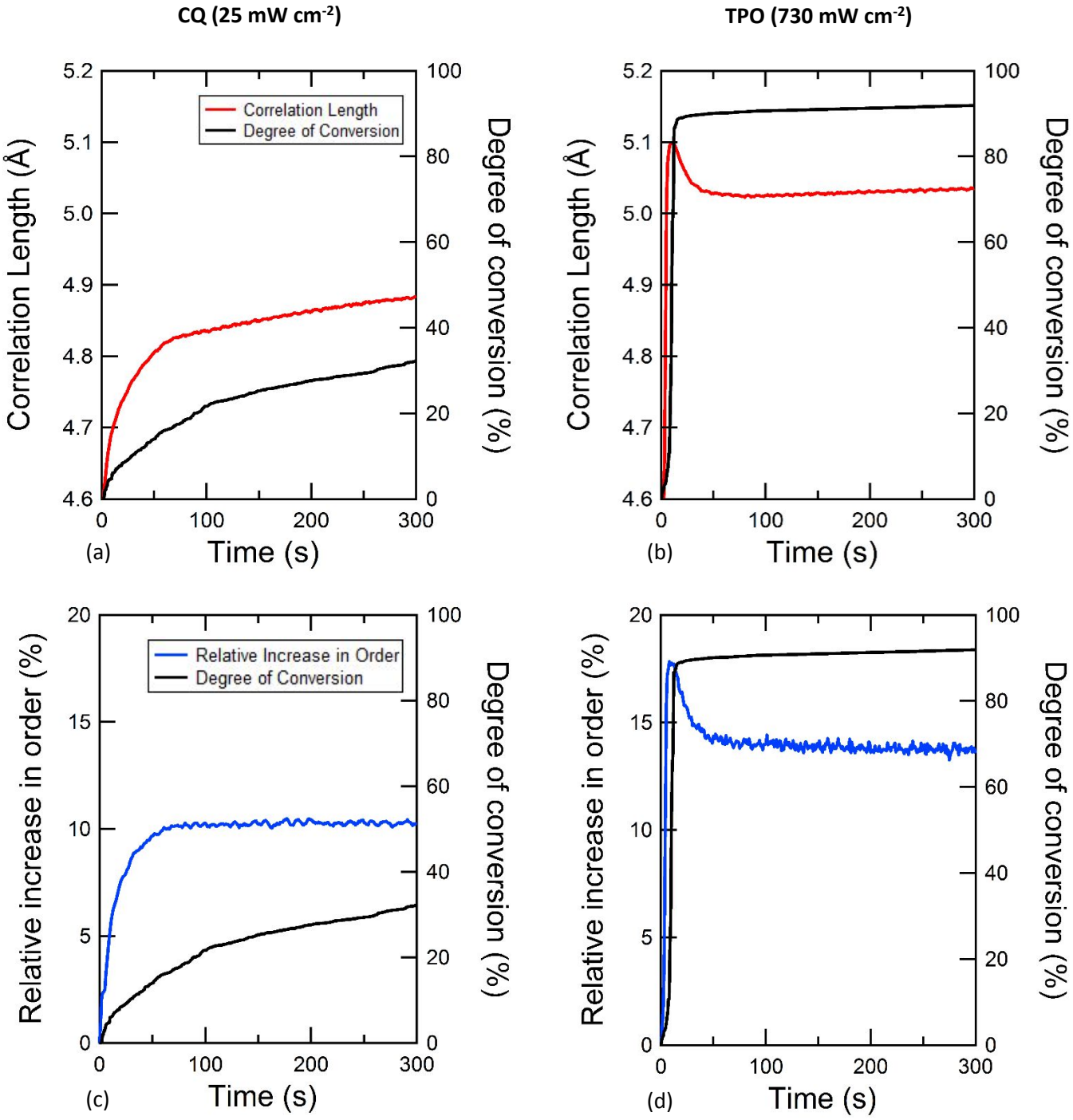

Figure 7. Representative plots of; **Top row:** Real time evolution of the correlation length observed in 50/50 wt% resin blends polymerised with either **(a)** CQ or **(b)** TPO photo-initiator at intensities of 25 and 730 mW cm^{-2} respectively. All resins display an increase in the correlation length which is larger and faster for higher polymerisation rates. For particularly fast reactions, a subsequent relaxation period can be seen after the initial increase in length **Bottom row:** The relative percentage increase in medium range structural order during photo-polymerisation for **(c)** low and **(d)** high irradiances for the same resin blends. Changes in order are similar and occur simultaneously to those observed in the correlation length for CQ initiated blends. Data were obtained from I22 (Diamond Light Source).

Figure 7 (**c** and **d**) shows the increase in relative structural order, which provides insight into the distributions of chemical bond lengths and angles for fast and slower polymerisation rates as a function of time. An initial increase in structural order to a local maximum occurs simultaneously with similar changes seen in the correlation length. Faster polymerisation corresponded to a larger and more rapid gain in structural order. Additionally, fast polymerised systems also demonstrated a relaxation in structural order (see supporting data, Figure S6) where approximately 5-15 % of the initial gain was lost, mirroring changes in the correlation length (see supporting data, Figure S5). Similarly, at slower reaction rates these systems display negligible or non-existent relaxation (see supporting data, Figures S3 and S4). Relative orders do not however show a post relaxation increase as was observed in the correlation length for all polymerisation rates, instead appearing to plateau (at least for the duration of the measurements). The final (measured) relative value of structural order was on average greater in resins containing a higher proportion of TEGDMA monomer (see supporting data, Figures S4 and S6). These less viscous systems also showed greater differences in the final relative structural order, for identical blends polymerised at different rates.

The relationship between functional end group conversion and structural changes in the polymer are outlined in **Figure 7** (black traces), where the data sets are overlaid for the respective polymerisation rates as a function of time. TPO initiated systems showed more rapid periods of initiation and propagation in comparison to the CQ based resins, reaching auto-deceleration earlier. Final conversion (DC_{max}) and polymerisation rate (Rp) are greater in resins polymerised using TPO initiation and/or high light intensities for each blend ($p<0.05$). The auto-acceleration period, particularly for TPO based systems, corresponds to the large initial increase in the correlation length and relative structural order i.e. as the polymer network grows, medium range structural order and length scales increase. When the system has reached 98% of the total reactive group conversion the correlation length and medium range structural order also reached a maximum for faster polymerised systems (**Figure 7b and d**). However, the end of auto-acceleration lagged behind the local maxima of the correlation length and structural order for the slower (CQ initiated) resin systems (**Figure 7a and c**). Post auto-deceleration cure appears to correspond to a continued increase in the correlation length.

Greater post auto-deceleration cure in slowly polymerised resins corresponded to a larger gradual gain in the correlation length following the initial increase, whilst resins cured rapidly showed negligible post auto-deceleration cure and changes in the correlation length. This slow continued polymerisation does not appear to affect the observed relaxation period or the plateau observed in the medium range structural order.

3.3. The effect of temperature variations on the evolving polymer structure

Figure 8a illustrates the real time temperature variations in representative 60/40 wt% resin blends initiated with either CQ or TPO during photo-polymerisation. A rapid increase in the temperature of the resin blend followed by a gradual decrease is observed for both photo-initiator systems. Resins initiated with TPO demonstrate a larger temperature increase in a shorter period of time compared with CQ based systems. Increases and relaxations in temperature during photo-polymerisation approximately coincide with similar behaviour seen in the correlation length (**Figure 7a** and **b**) and medium range order (**Figure 7c** and **d**) for the respective photo-initiator species despite differences in sample set up. **Figure 8b** shows the increase in correlation length and medium range order as a function of temperature for a pre-polymerised 60/40 wt% resin specimen. It can be seen that heating confers an almost linear extension of the correlation length at a rate of ~ 0.0016 ÅC$^{\circ-1}$, whilst order decreases by approximately 1.5 %.

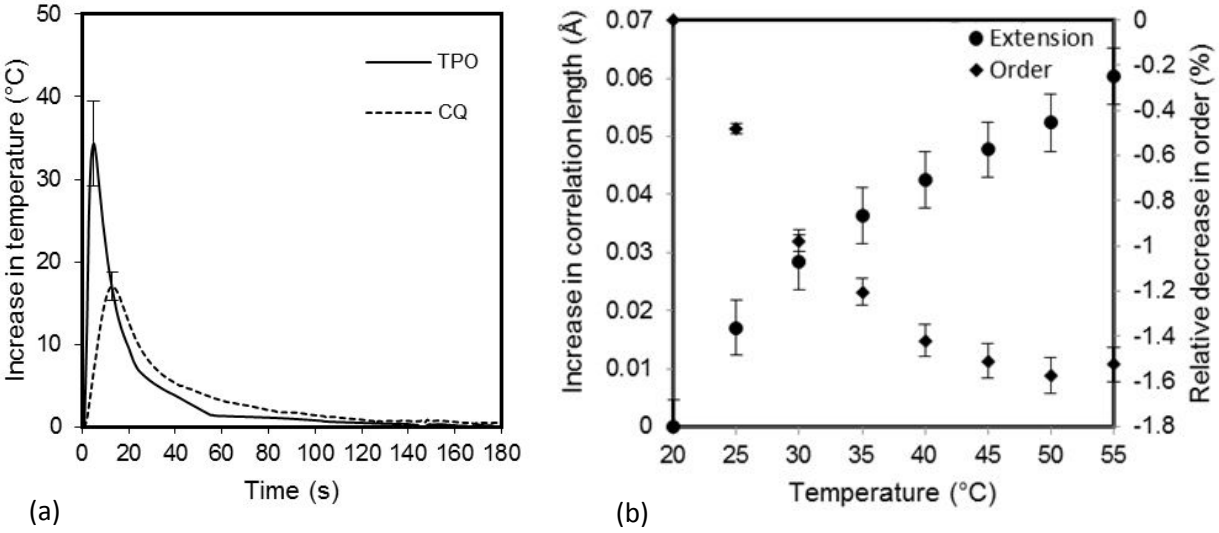

Figure 8. (a) Plot of the mean temperature rise (n=6) compensated for heating from the curing light, during photo-curing of 60/40 wt% Bis-GMA/TEGDMA monomer blends containing either a CQ or TPO photo-initiator. Error bars at peak temperature rise represent one standard deviation. **(b)** shows the mean relative increase and associated error bars, obtained from the propagation of errors of peak fitting uncertainties, in the X-ray scattering correlation length and order following controlled heating of pre-polymerized 60/40 wt% Bis-GMA/TEGDMA from 20 to 55 °C.

3.4. The effect of polymerisation rate on the resultant polymer structure

A range of polymerisation rates for each resin blend were achieved by varying photo-initiator chemistry and light irradiance and were characterised by FT-NIR. In **Figure 9** by correlating polymerisation rate with changes in X-ray scattering it was possible to relate reaction rate to (medium-range) structural evolution. As polymerisation rate increased there was a greater increase in the correlation length (extension) and relative medium range structural order. **Figure 9** demonstrates how systems initiated with Lucirin TPO (the last four data points) display polymerisation rates typically an order of magnitude greater than the CQ counterpart (the first four data points and inset in **Figure 9**) for similar irradiances. This conferred larger gains in the correlation length which were approximately twice those seen in CQ systems. At lower polymerisation rates (<5 % s^{-1}) the increase in the correlation length was observed to increase linearly with the polymerisation rate (**Figure 9**) however as the reaction rate increases the change in correlation length begins to plateau. More fluid resins, with a greater content of TEGDMA, displayed a greater increase in the correlation length for equivalent polymerisation rates. A similar relationship was observed when changes in medium range structural order were correlated with the polymerisation rate (see supporting data, Figure S8) albeit that the initial increases in relative order were much greater for the more fluid systems (greater TEGDMA %).

Direct correlations between X-ray data and the polymerisation rate are complicated by the relative differences in reactive group conversion for each polymerising system. Normalising the increase in correlation length with respect to DC_{max} resulted in a similar pattern of behaviour to that observed in **Figure 9**. However, normalising structural order to DC_{max} and plotting as a function of polymerisation rate (**Figure 10**) demonstrated that at polymerisation rates greater than ~5 % s^{-1} the gain in order decreases with increasing reaction rate for all resin blends. Relative structural order remained ranked by resin 'viscosity' with blends composed primarily of the Bis-GMA monomer demonstrating greater disorder at all polymerisation rates.

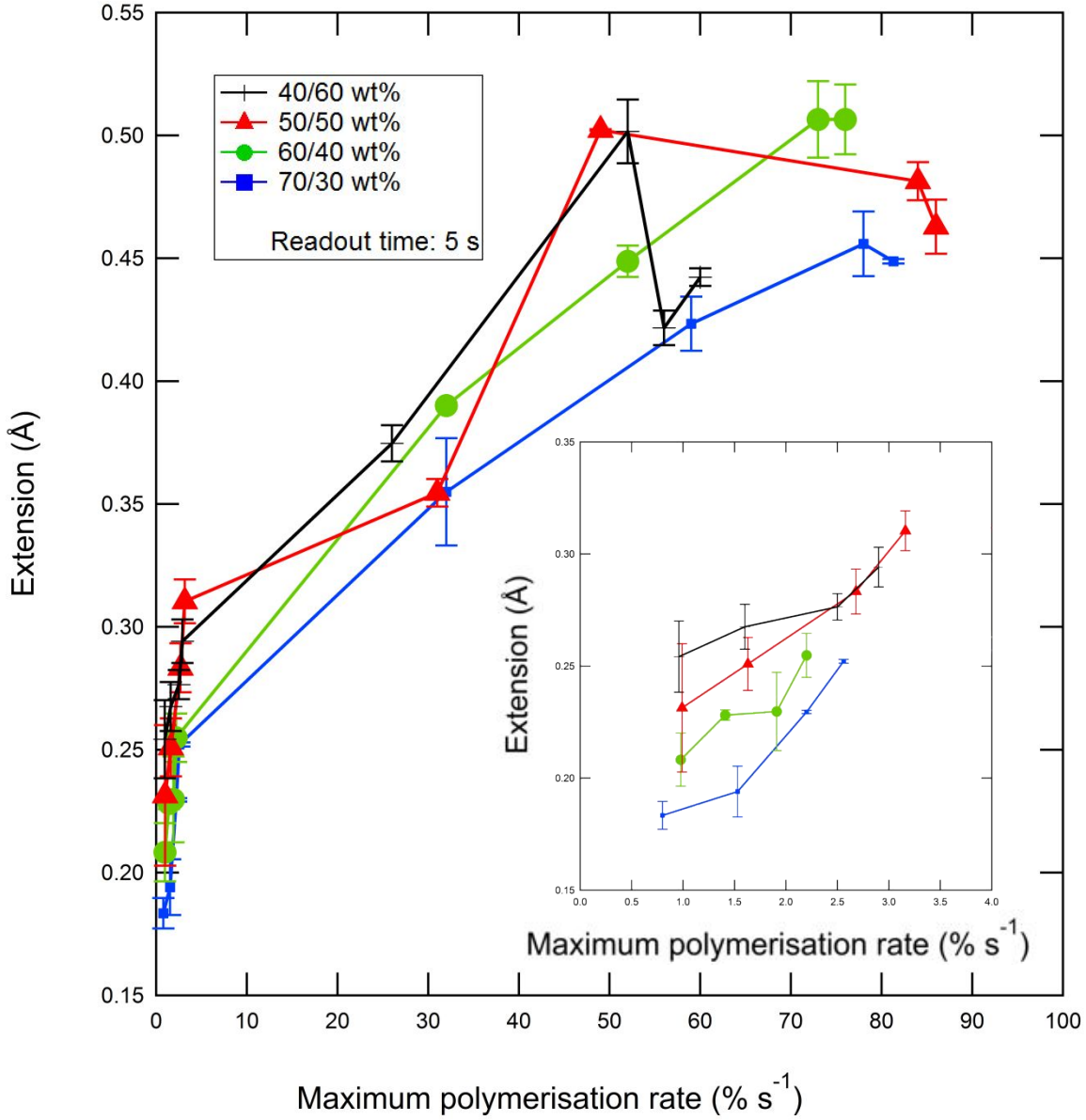

Figure 9. Maximum chain extension for each resin blend (viscosity) versus polymerisation rate (irradiance). The maximum extension was calculated as the difference between the initial and greatest values of the correlation length for each blend. CQ initiated resins are shown by the first four points and are also inset, whilst the other data points refer to TPO initiated resins. Resins polymerised at higher rates display the greatest increase in the correlation length. Data were obtained from BM28 (ESRF), see suporting materials and methods.

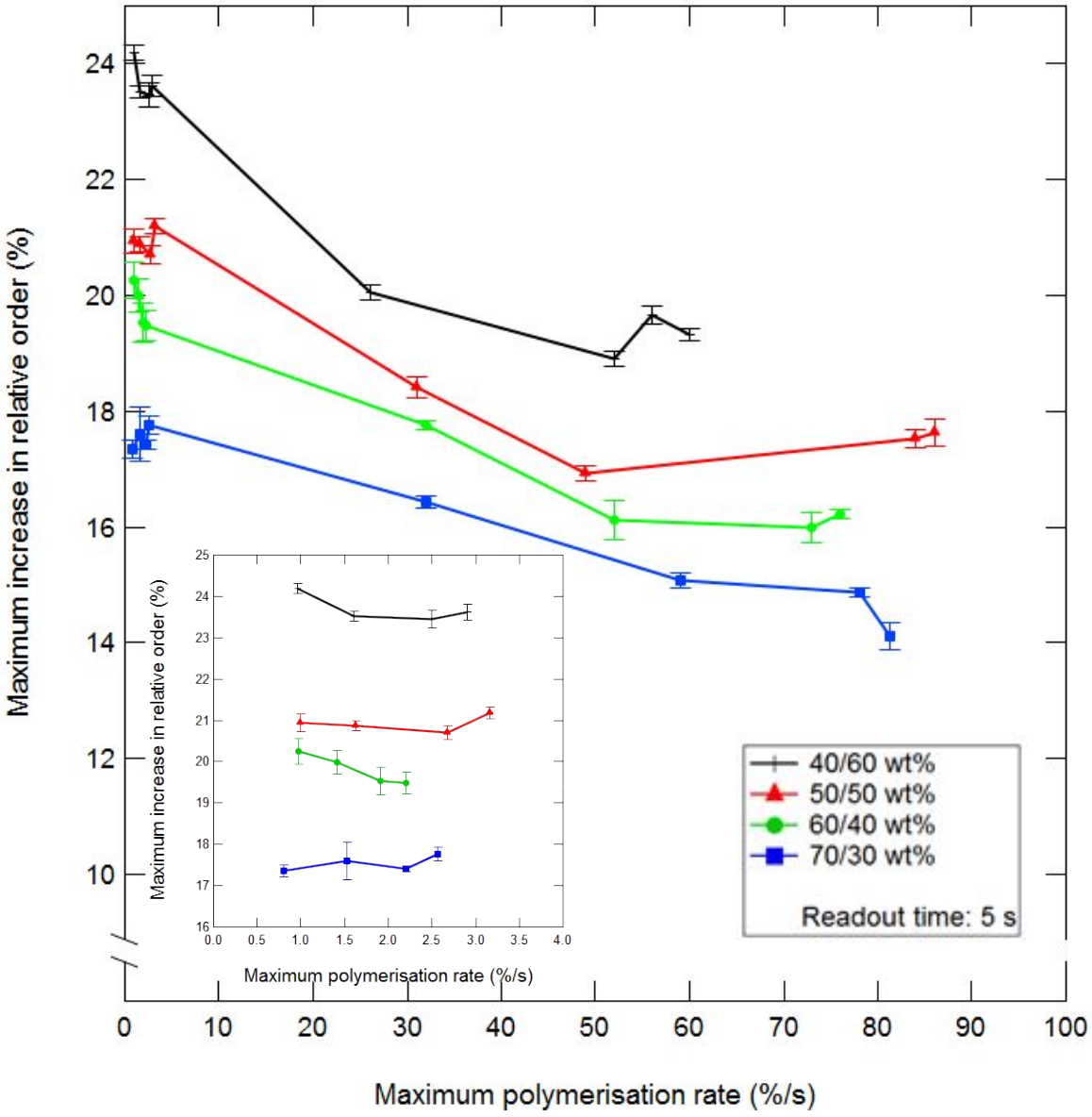

Figure 10. Normalised maximum increase in relative medium range structural order for each resin blend (viscosity) versus polymerisation rate (irradiance). Data has been normalised to the degree of reactive group conversion to determine chain extension and structural order per converted C=C bond. CQ initiated resins are shown by the first four points (also inset), whilst the other data points refer to TPO initiated resins. Systems polymerised at slower rates display the greatest increase in structural order for a given blend, whilst increasing viscosity decreases medium range order. Data were obtained from BM28 (ESRF), see supporting materials and methods.

4. DISCUSSION

4.1. De-convolving the contributions of monomeric components to the scattering signal

Photo-polymerisation induced an increase in the length of the principal X-ray scattering feature observed in measurements on the Bis-GMA/TEGDMA monomer blends (**Figure 3a**). Previous laboratory based measurements (WAXS) have measured this broad peak feature but have failed to determine its origin or explain the subtle differences in the peak position between resin blends of varying viscosities [38] which have been resolved here. In this study the correlation length increases from an initial value of ~ 4.45 Å up to ~ 5.1 Å (**Figures 3a, 7a and 7b**) depending on the resin formulation and the polymerisation rate. Weighted least squares fitting (WLS) of the scattering data for a 60/40 BisGMA/TEGDMA wt% blend, revealed that the majority of the length change originates from the TEGDMA monomer (**Figures 4** and **5**) and specifically within the methacrylate functional end groups (~48% of the total signal). The remaining portion of this length change is ascribed to the ether backbone in the TEGDMA monomer, which accounts for the remaining ~22% of the total signal.

The mechanism behind the length increase can be determined by considering that during polymerisation the C=C double bond in the methylene functional group is converted to a single covalent bond with a carbon atom from a neighbouring monomer. Bond conversion confers a length increase equivalent to 0.2 Å [the difference in bond length between a C=C bond (1.33 Å) and a C-C bond (1.53 Å)] [39] **Figures 7a and 9** show that for lower rates of polymerisation, less than 2 $\%s^{-1}$, the increases in the observed correlation length approximates the difference in length between double and single carbon–carbon bonds following polymerisation. This implies that at lower reaction rates the predominant form of length change arises from bond exchange. However, at higher reaction rates, in excess of 50 $\%s^{-1}$, the increase in the correlation length is more than double the bond exchange value (**Figures 7b and 9**). This additional increase in length, which cannot be accounted for through bond exchange, is therefore ascribed to chain segment extension. Fu *et al* (2015) [40] reported chain extension

in methacrylate functionalised monomers which were photo-initiated with UV light. However, the location(s) of the chain extension were not elucidated in their study.

Chain extension along the TEGDMA backbone is further supported by neutron scattering data from partially deuterated blends (**Figure 6**). **Figure 6** shows a broad scattering peak for a 60/40 wt% (Bis-GMA/d_{10}-TEGDMA) liquid monomer located at approximately 0.68 $Å^{-1}$ (~9.23 Å), which shifts to lower q and narrows following photo-polymerisation. This scattering peak is known to correspond to the correlation lengths between the deuterated portions of the functional end groups of d_{10}-TEGDMA, due to the absence of this scattering peak in a hydrocarbon functionality counterpart (**Figure 6**), and was synthesised specifically for this purpose. Therefore, this correlation length represents the approximate end to end vector distance of the d_{10}-TEGDMA monomer and gives insight into the structure of TEGDMA. The increase in the correlation length is also seen in the X-ray scattering data and exceeds that which could be attributed to bond exchange. The relatively small difference in the peak shift between the high and low irradiance polymerisation regimes for partially deuterated resins is attributed to fabricating the samples in advance of the neutron scattering measurements, due to the scheduling of experiments based at central facilities, which has likely permitted structural modifications to occur during a post cure period. Isotopic substitution of the functional end groups also prevents the quantification of DC_{max} to normalise changes in correlation length, which will likely reduce apparent differences in correlation length and structural order for identical systems polymerised with differences irradiances. Deuterated resins polymerised at lower irradiances demonstrated greater medium range order compared with higher irradiances similar to changes in order observed with X-ray scattering at shorter length scales. This strongly suggests that chain extension is the predominant mechanism for this length increase which occurs at sights distant from bond conversion/cross-links and at different length scales.

The Bis-GMA monomer also displays a smaller contribution to the total X-ray scattering signal (~30%) and subsequent q shift. Any extension arising from the Bis-GMA monomer is attributed solely to the non-aromatic portion of the monomer, including the functional end groups, given the rigidity of the aromatic rings at the centre of the monomer. No reports in the literature have indicated

structural changes to the aromatic groups via vibrational spectroscopy methods [4,41]. Microgel clusters will also inevitably form at longer length scales, although it is not possible to interpret structural properties over this range using standard X-ray/neutron scattering approaches due to the lack of clearly definable order. Optical scattering and computational modelling[42] may provide deeper insight into local density fluctuations. It must also be acknowledged that irradiance, DC and polymerisation rate will vary through the resin specimen as a function of sample thickness[43,44]. Therefore, any variation in the rate of reactive group conversion and hence chain extension is averaged by both FT-NIR spectroscopy and X-ray scattering measurements respectively. Additionally, the light source demonstrates high homogeneity and top hat factor such that lateral variation of irradiance over the face of the resin specimen is considered to be negligible

4.2. Impact of irradiance on the resultant polymer structure

Systems polymerised relatively slowly, which were typically CQ initiated resins and some TPO systems polymerised at low light intensities, demonstrated a gradual increase in the correlation length up to a gain of approximately 0.2 Å (**Figure 7a**). This is also accompanied by simultaneous increases in the medium range structural order during polymerisation, both of which are synchronised with the real time degree of conversion. Hence, polymerisation of the system confers an increase in the correlation length (corresponding to segments within a monomeric unit) and medium range structural order. In **Figure 7a**, a gradual increase in correlation length is observed representing an increasing contribution of the longer correlation lengths (arising from increasing C=C to C-C conversion) to the average scattering signal. It can be seen that medium range structural order also displays a similar initial increase which coincides with polymerisation (**Figure 7c**) and is attributed to bond conversion. It is known that polymerisation limits the range of monomer motion at the end groups which reduces the number of possible bond conformations [45]. **Figure 7a** shows that the local maxima in the correlation length correspond to plateauing of *DC*. Additionally, the gain in the correlation length consistently exceeds 0.2 Å after a small reversal in extension feature which may represent a transition from chain growth induced length changes to true chain extension. In systems polymerised at relatively slow rates the maximum rate of conversion (R_{pmax}) occurs at lower reactive group

conversion[46,47]. A smaller fraction of monomer/polymer segments are perturbed at this point in the reaction, the relaxation time of polymer segments (τ) is significantly less than the rate of conversion[46] (R_p) i.e. $\tau << R_p$ and fewer segments are stored in a higher energy conformation within the forming network. After this point in the reaction $\tau < R_p$, so the polymer segments have more time to extend and reorientate to achieve greater structural order. Therefore, chain extension in relatively slowly polymerised resins seems to occur after the majority of the cross-linked network has been formed.

At faster polymerisation rates (**Figures 7b and d**) greater increases in the correlation length and order in a shorter period of time are observed. At higher rates (TPO, high irradiance) the increase in the correlation length is more than double of that than can be ascribed to bond-exchange (associated with chain growth) and is followed by a relatively large reduction in extension length, proportional to the initial length increase. Rapid heating and cooling (**Figure 8a**) coincides with a large gain and relaxation in the correlation length and order, particularly for systems polymerised at faster rates through the use of higher irradiance and/or TPO photo-initiator. Thermal data indicates a strong likelihood that this temperature rise during photo-polymerisation in the resin contributes to the chain extension peak/relaxation seen at early time points. In particular, the peak temperature closely matches the limit of peak extension at R_{pmax}. However, *in-situ* heating/X-ray scattering measurements suggest this temperature rise may not account entirely for the extension/relaxation behaviour of the polymer segments at these early time points. **Figure 8b** demonstrates that a greater temperature increase than seen during polymerisation (**Figure 8a**) would be required to confer the magnitude of chain extension reported in **Figure 9**. Furthermore, the gradual decrease in order (**Figure 7d**) occurs as the resin cools (**Figure 8a**), yet cooling would be expected to produce a relative increase in order as polymer thermal motions are reduced. This relationship is confirmed in **Figure 8b** where heating of a 60/40 wt% resin conferred a relative decrease in order. A relaxation in order therefore supports the assertion that rapid polymerisation and polymer growth generates stress within monomeric units, causing extension of segments (more so than for systems polymerised with lower reaction rates). Relaxation of these length scales may therefore represent a reorientation of bond geometry to lower the energy state of the system i.e. stress relief within the polymer structure.

Figure 7b also shows that systems polymerised rapidly can demonstrate varying degrees of chain extension post-relaxation. This feature is most prominent in systems polymerised using lower light intensities, achieving lower conversion (see supporting data, Figure S3). In comparison, a system which has been polymerised rapidly and has reached a high terminal conversion displays negligible extension after the initial increase and subsequent reduction in correlation length (see supporting data, Figure S5). Any changes in correlation length after gelation are attributed to continued conversion i.e. bond exchange. Post-cure will be associated with polymerisation with less geometric freedom for the reacting monomer. This restriction of geometric freedom is likely to lead to bond and chain geometries that are longer than a comparative unconstrained state and leads to the net increase in correlation lengths seen at extended times for systems with initially lower *DC*.

At lower *DC* more free volume is likely to be available and diffusion limits do not fully restrict the movement of radical species. This allows for continued conversion of reactive groups (**Figure 7a**) which causes the monomer segment to incrementally extend. Resins polymerised rapidly with a greater terminal degree of conversion (> 90%) will demonstrate little final free volume. This limited mobility restricts further structural modifications such that an extended chain conformation is fixed into the polymer network. To summarise, at greater polymerisation rates R_{pmax} will occur at greater values of conversion[46,47] and a larger fraction of polymer segments will be perturbed. Here, $\tau << R_{pmax}$ and the polymer segments will have insufficient time to relax[46,47] following chain extension. Consequently, higher energy (possibly under strain) extended chain segment conformations are stored within the network structure whilst the cross-linked network forms and the resultant structures are unable to undergo further modifications post auto-deceleration with respect to medium range structural order due to mobility restrictions.

4.3. The effect of polymerisation rate on the resultant polymer structure

It can be seen from **Figure 9** that as the polymerisation rate is increased there is a greater increase in the correlation length (extension). At lower polymerisation rates (less than 2 $\%s^{-1}$) the relationship between extension and rate is linear, however above this threshold the extension begins to plateau. This plateau in extension at higher rates may represent either the maximum extension of the monomer segment i.e. towards an ideal conformation or alternatively the maximum length before solidification restricts further extension. A similar pattern is observed when changes in medium range structural order were correlated with the polymerisation rate (see supporting data, Figure S8). Greater relative structural order in resins polymerised using a fast rate is likely an effect of differences in reactive group conversion. A more polymerised system will inevitably display greater structural order due to the restriction of the thermal motions and chemical bond distributions.

Direct correlations between X-ray scattering data and the polymerisation rate are therefore complicated by the relative differences in reactive group conversion for each polymerising system. Degree of conversion was quantified using both real time *ex-situ* laboratory based FT-NIR spectroscopy and *in-situ* measurements performed simultaneously to the acquisition of X-ray data with differences between the two measurements considered negligible. Normalising the increase in correlation length with respect to *DC* resulted in a similar pattern of observations to those seen in **Figure 9** (see supporting data, Figure S7). However, **Figure 10** shows that normalised structural order decreases with increasing reaction rate. This implies that driving the polymerisation rate faster reduces the amount of time that the monomeric structure has to reorient and optimise its bond geometry during network growth. At slower polymerisation rates, more time is allowed to achieve a lower energy (a more ordered) conformation.

The generation of macroscopic shrinkage [48] associated with the reduction of free volume during the polymerisation of these materials must be considered when interpreting these results. When shrinkage is constrained, the result is the generation of residual stress which will likely impact on the observed correlation lengths within the polymer system. The geometry of the test specimens used in this study

were largely unconstrained with a large aspect ratio between the disc surface and the sample holder, with a readily deformable mica window. Although shrinkage has not been measured in this study, residual shrinkage strains would manifest as increased correlation lengths that may relax over time. When polymerisation is accelerated through the use of TPO initiator and the highest irradiance a relaxation feature is observed. It is conceivable that this feature is a form of stress relief mechanism, such as bond exchange or breakage.

5. CONCLUSIONS

The evolving polymer structure of photo-activated dimethacrylate resins has been studied using neutron scattering, time resolved X-ray scattering, and *in-situ* FT-NIR spectroscopy as a function of polymerisation rate. Photo-polymerisation induces structural changes in the monomeric units with regards to chain segment extension and relative structural order which to date is unreported for these materials. It appears that chain extension occurs predominantly in the methacrylate functional groups of Bis-GMA and TEGDMA monomer, although extension also occurs in the ether backbone of the TEGDMA monomer. Faster polymerisation rates generate greater extension in a shorter period of time and as a consequence the developing structure has less time to orient to a lower energy (higher order) conformation. By polymerising the system rapidly, to the point of solidification, any residual stresses generated by chain extension remain fixed into the polymer network. In comparison, slowly polymerised systems are capable of modifying the polymer structure after the majority of the network has formed, which is most likely due to a greater availability of free volume. This series of experiments within the context of the photo-polymerisation of biomedical resins has shown how operator-induced, environmental and compositional variables may impact polymerisation. This may ultimately explain the discrepancies in the predictive modelling of the mechanical behaviour of these materials used in this field to date.

Contributions

O.A, R.A.M, M.W.A.S and S.S conceived the experiment, performed the measurements, interpreted the data and drafted the manuscript. Y.G conducted thermal analysis. M.P synthesised the d_{10}-TEGDMA. P.B.J.T, A.J.S and W.M.P assisted with measurements and interpreting data. All authors revised the manuscript prior to submission.

Funding sources

The following funding is acknowledged: Science and Technology Facilities Council (award No. ST/L502510/1) and the Royal College of Surgeons of England Small Grants Scheme (Faculty of Dental Surgery)

Competing interests

The authors declare no competing interests.

Acknowledgements

The authors would like to thank Diamond Light Source for beam time (proposals SM11687-1 and SM14117) and the staff of the I22 beamline for their assistance with data collection. We thank the Science and Technology Facilities Council (STFC) for access to the SANS2D neutron beamline (proposal 1320128) at ISIS. We also acknowledge the European Synchrotron Radiation Facility for provision of synchrotron radiation facilities (proposals 28-01-1059 and 28-01-1025) and the institute Laue Langevin (proposal 9-11-1714) and the staff of the BM28 and D16 beamlines respectively for their assistance with data collection.

Supporting information. Description of d_{10}-TEGDMA synthesis. Outline of additional time resolved X-ray scattering experiment conducted at BM28 ESRF (Grenoble, France). Real time evolution of the correlation length and change in relative structural order observed in CQ and TPO initiated resins. Maximum chain extension for each resin blend normalised to the degree of reactive

group conversion, versus polymerisation rate. Maximum increases in structural order for each resin blend versus polymerisation rate.

REFERENCES

(1) Calheiros, F. C.; Kawano, Y.; Stansbury, J. W.; Braga, R. R. Influence of Radiant Exposure on Contraction Stress, Degree of Conversion and Mechanical Properties of Resin Composites. *Dent. Mater.* **2006**, *22* (9), 799–803.

(2) Stansbury, J. W. Dimethacrylate Network Formation and Polymer Property Evolution as Determined by the Selection of Monomers and Curing Conditions. *Dent. Mater.* **2012**, *28* (1), 13–22.

(3) Ogunyinka, A.; Palin, W. M.; Shortall, A. C.; Marquis, P. M. Photoinitiation Chemistry Affects Light Transmission and Degree of Conversion of Curing Experimental Dental Resin Composites. *Dent. Mater.* **2007**, *23* (7), 807–813.

(4) Stansbury, J. W.; Dickens, S. H. Determination of Double Bond Conversion in Dental Resins by near Infrared Spectroscopy. *Dent. Mater.* **2001**, *17* (1), 71–79.

(5) Dickens, S. H.; Stansbury, J. W.; Choi, K. M.; Floyd, C. J. E. Photopolymerization Kinetics of Methacrylate Dental Resins. *Macromolecules* **2003**, *36* (16), 6043–6053.

(6) Ruyter, I. E.; Oysaed, H. Composites for Use in Posterior Teeth: Composition and Conversion. *J. Biomed. Mater. Res.* **1987**, *21* (1), 11–23.

(7) Ferracane, J. L. Current Trends in Dental Composites. *Crit. Rev. Oral Biol. Med.* **1995**, *6* (4), 302–318.

(8) Lima, A. F.; de Andrade, K. M. G.; da Cruz Alves, L. E.; Soares, G. P.; Marchi, G. M.; Aguiar, F. H. B.; Peris, A. R.; Mitsui, F. H. O. Influence of Light Source and Extended Time of Curing on Microhardness and Degree of Conversion of Different Regions of a Nanofilled Composite Resin. *Eur. J. Dent.* **2012**, *6* (2), 153–157.

(9) Peutzfeldt, A.; Asmussen, E. The Effect of Postcuring on Quantity of Remaining Double Bonds, Mechanical Properties, and in Vitro Wear of Two Resin Composites. *J. Dent.* **2000**, *28* (6), 447–452.

(10) Feng, L.; Byoung, I. S. Exposure Reciprocity Law in Photopolymerization of Multi-Functional Acrylates and Methacrylates. *Macromol. Chem. Phys.* **2007**, *208* (3), 295–306.

(11) Emami, N.; Söderholm, K. J. How Light Irradiance and Curing Time Affect Monomer Conversion in Light-cured Resin Composites. *Eur. J. Oral Sci.* **2003**, *111* (6), 536–542.

(12) Halvorson, R. H.; Erickson, R. L.; Davidson, C. L. Energy Dependent Polymerization of Resin-Based Composite. *Dent. Mater.* **2002**, *18* (6), 463–469.

(13) Sakaguchi, R. L.; Ferracane, J. L. Effect of Light Power Density on Development of Elastic Modulus of a Model Light-Activated Composite during Polymerization. *J. Esthet. Restor. Dent.* **2001**, *13* (2), 121–130.

(14) Lovell, L. G.; Lu, H.; Elliott, J. E.; Stansbury, J. W.; Bowman, C. N. The Effect of Cure Rate on the Mechanical Properties of Dental Resins. *Dent. Mater.* **2001**, *17* (6), 504–511.

(15) Wydra, J. W.; Cramer, N. B.; Stansbury, J. W.; Bowman, C. N. The Reciprocity Law Concerning Light Dose-Relationships Applied to BisGMA/TEGDMA Photopolymers: Theoretical Analysis and Experimental Characterization. *Dent. Mater*. **2014**, *30*(6):605-12.

(16) Sideridou, I.; Tserki, V.; Papanastasiou, G. Effect of Chemical Structure on Degree of Conversion in Light-Cured Dimethacrylate-Based Dental Resins. *Biomaterials* **2002**, *23* (8), 1819–1829.

(17) Van Landuyt, K. L.; Snauwaert, J.; De Munck, J.; Peumans, M.; Yoshida, Y.; Poitevin, A.; Coutinho, E.; Suzuki, K.; Lambrechts, P.; Van Meerbeek, B. Systematic Review of the Chemical Composition of Contemporary Dental Adhesives. *Biomaterials* **2007**, *28* (26), 3757–3785.

(18) Venhoven, B. A.; de Gee, A. J.; Davidson, C. L. Light Initiation of Dental Resins: Dynamics of the Polymerization. *Biomaterials* **1996**, *17* (24), 2313–2318.

(19) Lovell, L. G.; Stansbury, J. W.; Syrpes, D. C.; Bowman, C. N. Effects of Composition and Reactivity on the Reaction Kinetics of Dimethacrylate/Dimethacrylate Copolymerizations. *Macromolecules* **1999**, *32* (12), 3913–3921.

(20) Amirouche-Korichi, A.; Mouzali, M.; Watts, D. C. Effects of Monomer Ratios and Highly Radiopaque Fillers on Degree of Conversion and Shrinkage-Strain of Dental Resin Composites. *Dent. Mater.* **2009**, *25* (11), 1411–1418.

(21) Chen, Y.-C.; Ferracane, J. L.; Prahl, S. A. Quantum Yield of Conversion of the Photoinitiator

Camphorquinone. *Dent. Mater.* **2007**, *23* (6), 655–664.

(22) Nie, J.; Andrzejewska, E.; Rabek, J.F.; Lindén, L. Å.; Fouassier, J. P.; Paczkowski, J.; Scigalski, F.; Wrzyszczynski, A. Effect of Peroxides and Hydroperoxides on the Camphorquinone-initiated Photopolymerization. *Macromol. Chem. Phys.* **1999**, *200* (7), 1692–1701.

(23) Monroe, B. M.; Weiner, S. A.; Hammond, G. S. Mechanisms of Photochemical Reactions in Solution. LII. Photoreduction of Camphorquinone. *J. Am. Chem. Soc.* **1968**, *90* (7), 1913–1914.

(24) Peutzfeldt, A.; Asmussen, E. Resin Composite Properties and Energy Density of Light Cure. *J. Dent. Res.* **2005**, *84* (7), 659–662.

(25) Miyazaki, M.; Oshida, Y.; Keith Moore, B.; Onose, H. Effect of Light Exposure on Fracture Toughness and Flexural Strength of Light-Cured Composites. *Dent. Mater.* **1996**, *12* (5), 328–332.

(26) Erik, A.; Anne, P. Polymerization Contraction of Resin Composite vs. Energy and Power Density of Light-cure. *Eur. J. Oral Sci.* **2005**, *113* (5), 417–421.

(27) Feng, L.; Carvalho, R.; Suh, B. I. Insufficient Cure under the Condition of High Irradiance and Short Irradiation Time. *Dent. Mater.* **2009**, *25* (3), 283–289.

(28) Simmons, C. J.; El-Bayoumi, O. H. *Experimental Techniques of Glass Science*; J. Am. Ceram. Soc. 1993.

(29) Ellakwa, A.; Cho, N.; Lee, I. B. The Effect of Resin Matrix Composition on the Polymerization Shrinkage and Rheological Properties of Experimental Dental Composites. *Dent. Mater.* **2007**, *23* (10), 1229–1235.

(30) Sears, V. F. Neutron Scattering Lengths and Cross Sections. *Neutron News* **1992**, *3* (3), 26–37.

(31) Stahl, F.; Ashworth, S. H.; Jandt, K. D.; Mills, R. W. Light-Emitting Diode (LED) Polymerisation of Dental Composites: Flexural Properties and Polymerisation Potential. *Biomaterials* **2000**, *21* (13), 1379–1385.

(32) Basham, M.; Filik, J.; Wharmby, M. T.; Chang, P. C. Y.; El Kassaby, B.; Gerring, M.; Aishima, J.; Levik, K.; Pulford, B. C. A.; Sikharulidze, I.; et al. Data Analysis WorkbeNch

(DAWN). *J. Synchrotron Radiat.* **2015**, *22* (Pt 3), 853–858.

(33) Filik, J.; Ashton, A.; C Y Chang, P.; A Chater, P.; J Day, S.; Drakopoulos, M.; Gerring, M.; Hart, M.; Magdysyuk, O.; Michalik, S.; et al. Processing Two-Dimensional X-Ray Diffraction and Small-Angle Scattering Data in DAWN 2. *J. Appl. Crystallogr.* **2017**; 50, 959-966

(34) Heenan, R.; King, S.; Turner, D. S.; Treadgold, J. R. SANS2D at the ISIS Second Target Station. *Proc. ICANS-XVII,* **2006**, 780-785.

(35) Duxbury, D.; Heenan, R.; McPhail, R.; Raspino, D.; Rhodes, N.; Rodgers, S.; Schooneveld, E.; Spill, E.; Terry, A. Performance Characteristics of the New Detector Array for the SANS2d Instrument on the ISIS Spallation Neutron Source. *J. Instrum.* **2014**, *9* (12), C12051.

(36) Arnold, O.; Bilheux, J. C.; Borreguero, J. M.; Buts, A.; Campbell, S. I.; Chapon, L.; Doucet, M.; Draper, N.; Ferraz Leal, R.; Gigg, M. A.; et al. Mantid—Data Analysis and Visualization Package for Neutron Scattering and μ SR Experiments. *Nucl. Instruments Methods Phys. Res. Sect. A Accel. Spectrometers, Detect. Assoc. Equip.* **2014**, *764*, 156–166.

(37) Collins, S. P.; Bombardi, A.; Marshall, A. R.; Williams, J. H.; Barlow, G.; Day, A. G.; Pearson, M. R.; Woolliscroft, R. J.; Walton, R. D.; Beutier, G.; et al. Diamond Beamline I16 (Materials & Magnetism). *AIP Conf. Proc.* **2010**, *1234* (1), 303–306.

(38) Fong, H.; Dickens, S. H.; Flaim, G. M. Evaluation of Dental Restorative Composites Containing Polyhedral Oligomeric Silsesquioxane Methacrylate. *Dent. Mater.* **2005**, *21* (6), 520–529.

(39) Cottrell, T. L. *The Strengths of Chemical Bonds*; Butterworth, London, 1961.

(40) Fu, Q.; McKenzie, T. G.; Tan, S.; Nam, E.; Qiao, G. G. Tertiary Amine Catalyzed Photo-Induced Controlled Radical Polymerization of Methacrylates. *Polym. Chem.* **2015**, *6* (30), 5362–5368.

(41) Rueggeberg, F. A.; Hashinger, D. T.; Fairhurst, C. W. Calibration of FTIR Conversion Analysis of Contemporary Dental Resin Composites. *Dent. Mater.* **1990**, *6* (4), 241–249.

(42) Sarkar, S.; Baker, P. J.; Chan, E. P.; Lin-Gibson, S.; Chiang, M. Y. M. Quantifying the Sensitivity of the Network Structure and Properties from Simultaneous Measurements during Photopolymerization. *Soft Matter* **2017**, *13* (21), 3975–3983.

(43) Chen, Y.-C.; Ferracane, J. L.; Prahl, S. A. A Pilot Study of a Simple Photon Migration Model for Predicting Depth of Cure in Dental Composite. *Dent. Mater.* **2005**, *21* (11), 1075–1086.

(44) Leprince, J. G.; Leveque, P.; Nysten, B.; Gallez, B.; Devaux, J.; Leloup, G. New Insight into the "Depth of Cure" of Dimethacrylate-Based Dental Composites. *Dent. Mater.* **2012**, *28* (5), 512–520.

(45) Darvell, B. W. Chapter 5 - Acrylic. In *Materials Science for Dentistry (Ninth edition)*; Darvell, B. W., Ed.; Woodhead Publishing Series in Biomaterials; Woodhead Publishing, 2009; pp 108–127.

(46) Anseth, K. S.; Kline, L. M.; Walker, T. A.; Anderson, K. J.; Bowman, C. N. Reaction Kinetics and Volume Relaxation during Polymerizations of Multiethylene Glycol Dimethacrylates. *Macromolecules* **1995**, *28* (7), 2491–2499.

(47) Cook, W. D. Photopolymerization Kinetics of Oligo(Ethylene Oxide) and Oligo(Methylene) Oxide Dimethacrylates. *J. Polym. Sci. Part A Polym. Chem.* **1993**, *31* (4), 1053–1067.

(48) Palin, W. M.; Hadis, M. A.; Leprince, J. G.; Leloup, G.; Boland, L.; Fleming, G. J. P.; Krastl, G.; Watts, D. C. Reduced Polymerization Stress of MAPO-Containing Resin Composites with Increased Curing Speed, Degree of Conversion and Mechanical Properties. *Dent. Mater.* **2014**, *30* (5), 507–516.

Supporting Materials and Methods

Synthesis of partially deuterated d_{10}-TEGDMA

Initially, diol (triethylene glycol) (3.5g, 23 mmol) in 80 mL of methylene chloride and 5.2 g (51 mmol) triethylamine (TEA) were mixed under a nitrogen atmosphere in an ice bath. Subsequently, 5.3 g (51 mmol, 10 % excess with respect to the diol) of undeuterated methacryloyl chloride in 20 mL of methylene chloride was added dropwise to the mixture during 1 hr, and the temperature was kept at -5°C. The reaction mixture was allowed to stir for two further hours at room temperature, and then was filtrated and treated with a 1 M HCl solution (2 × 40 mL), a saturated $NaHCO_3$ solution (2 × 40 mL), and distilled water (1 × 20 mL). The organic phase was dried with Na_2SO_4, and the solvent was evaporated to obtain a colorless liquid (TEGDMA).

The d_{10}-TEGDMA was synthesized according to the above procedure using undeuterated triethylene glycol (3g, 20 mmol), deuterated methacryloyl chloride-d_5 (5g, 45 mmol), and TEA (4.6g, 45 mmol). Because of the initially low yield (< 20%) the reaction time was extended to 8 h. The raw product was purified using column chromatography (1 × DCM/MeOH, 95/5, v/v, and 1 × chloroform), and then discolored with the use of activated carbon in diethyl ether. The overall yield was 35-40%. The product was stabilized with 100 ppm hydroquinone. The reaction process is summarized in **Figure S1**.

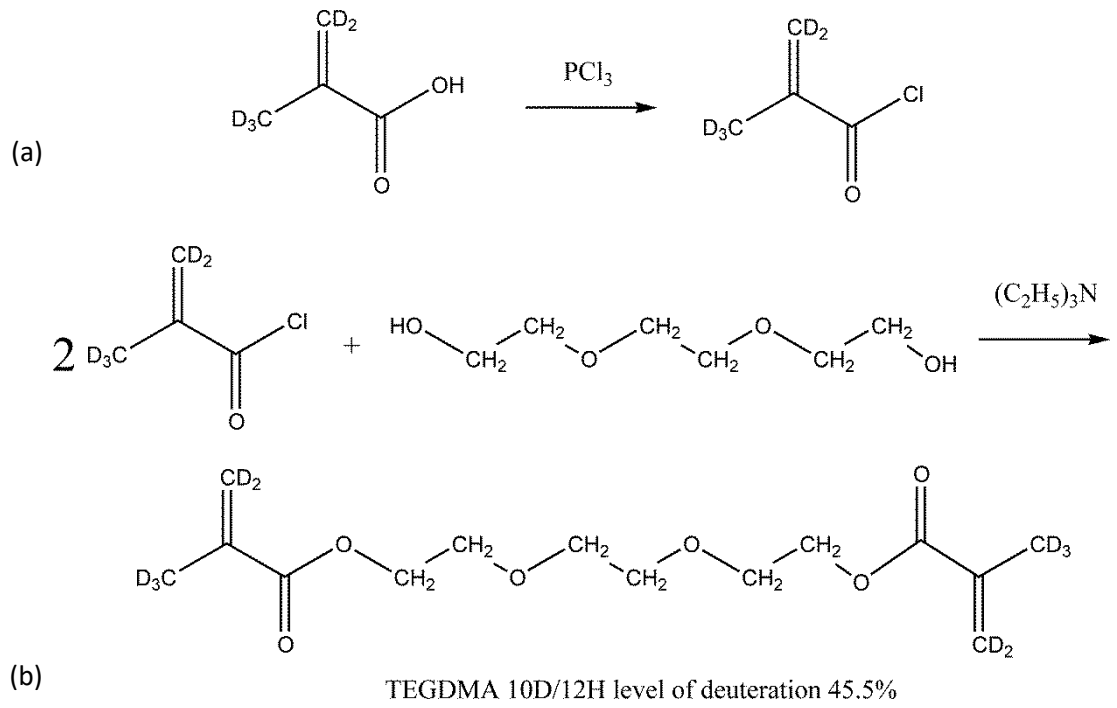

Figure S1. (a) Deuterated methacrylic acid combined with phosphorus trichloride in preparation for combining with triethylene glycol. **(b)** Combining deuterated methcroyl chloride with triethylene glycol to yield a partially deuterated TEGDMA monomer with 45.5% deuteration by molecular weight of the original hydrogen atoms.

FTIR spectra showed peaks at (cm^{-1}): 3010-2775 ($CH_{aliphatic}$), 1715 (CO), 1647 (residue $=CH_2$), 1595 ($=CD_2$), 1500-775 ($CH_{aliphatic}$), 1068 (CD), 745 (residue DCM). No alcohol or chloride IR peaks were detected after purification (**Figure S2**).

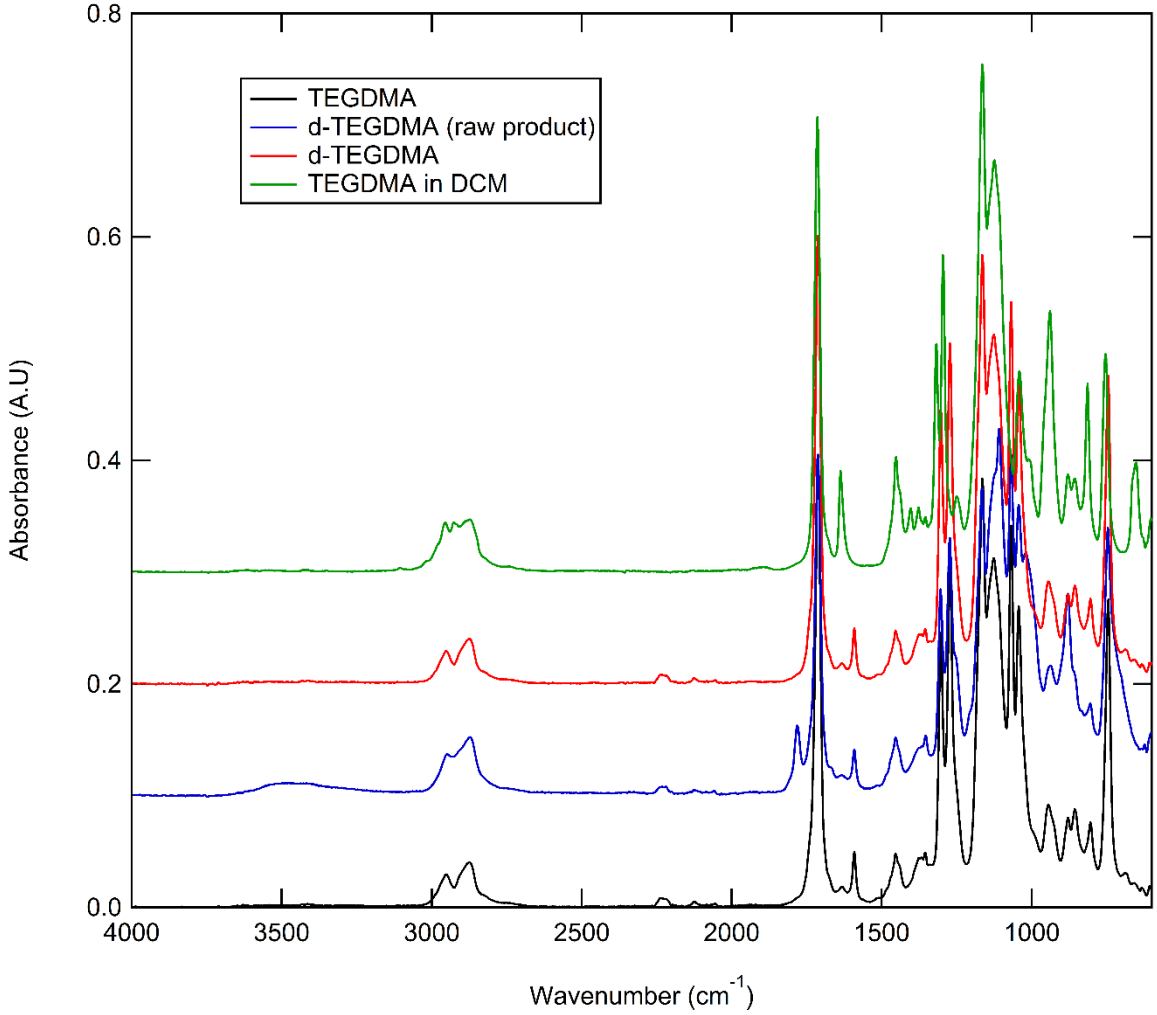

Figure S2. FTIR spectra for deuterated and undeuterated variants of the TEGDMA monomer. Spectra for the d_{10}-TEGDMA at specific steps of purification are also shown and are offset in the absorbance axis for clarity.

Synchrotron X-ray scattering measurements

Synchrotron X-ray scattering experiments were carried out on the XMaS beamline (BM28) at the European Synchrotron Radiation Facility (ESRF, Grenoble, France). An incident X-ray energy of 15 keV was used corresponding to a wavelength (λ) of 0.82 Å, with a beam size of 0.08 × 0.5 mm (horizontal × vertical) defined by vacuum tube slits. Measurements were carried out in air, at 23 ± 1 °C with light excluded other than the photo-curing light source.

Test specimens were prepared by filling a 0.9 mm thick stainless steel ring with a 10 mm internal diameter which was sealed on both faces by 25 μm thick Mylar film (RS, Northants, UK). The resin filled rings were housed within a brass block annulus (Daresbury Laboratory, Warrington, UK) and mounted at 30° normal to the path of the incident X-rays, 300 mm from the X-ray source. A 5 mm diameter light guide (Lumencor, Kent, UK) was fixed normal to and 10 mm distant from the centre of the resin surface and connected to a multichannel light source (Lumencor Aura Light engine, Lumencor, Kent, UK) to illuminate the sample.

For the TPO initiated resins, the light engine was programmed to emit a peak emission spectrum at 405 nm, whilst for CQ systems a wavelength of 470 nm was employed. The wavelengths of light were chosen to match the maxima in the absorption spectra of the respective photo-initiators. For each unique composition, samples of monomer blends were photo-polymerised at four different irradiances for each wavelength controlled by the power output of the light engine (5, 20, 60 and 100% power output) for a total of 300 s. Irradiances were calculated by spectrometry measurements for each experimental set-up, for each light source and power setting.

2D scattering images were collected using a 2048×2048 pixel MAR CCD (MAR CCD 165, Rayonix, Norderstedt, Germany) camera, 570 mm from the sample to give a q range of 0.1 to 1.9 $Å^{-1}$, where $q=4\pi \sin\theta/\lambda$. A Helium filled flight tube was employed to minimise air scattering. Scattering images were collected with a 1 s count time and a 4 s readout time giving a 5 s temporal resolution. Time resolved scattering measurements were conducted for each resin-blend by initially collecting data for

20 s prior to remote activation of the light engine. In addition to the time resolved photo-activated samples, X-ray measurements were acquired for the constituent monomers (Bis-GMA and TEGDMA) in isolation and containing photo-initiator to identify their contributions to the scattering signal of each blend. The contribution of the X-ray beam to the measurements was assessed by conducting observations for over 30 min for the uncured and polymerised samples in the absence of light. To aid data analysis measurements were taken for direct beam, empty sample containers, Mylar windows, water and a silver behenate calibration standard to allow the scattering patterns to be corrected for background and normalisation effects. Transmitted beam was recorded throughout using a beam-stop mounted photodiode. Data were normalised to the incident monitor intensity and background corrected using the Fit2D software package (version 12.077, ESRF, Grenoble, France). Data were azimuthally integrated over 360° to produce a 1D output and were subsequently fitted with a pseudo-Voigt model to determine peak positions and relative order.

Ex-situ Fourier Transform near infrared spectroscopy

Laboratory-based Fourier Transform Near Infrared (FT-NIR) Spectroscopy was used to determine the reaction rate and DC_{max} for each resin blend. All sample curing protocols used in X-ray scattering measurements at BM28 were reproduced in the laboratory using identical sample geometries, sample containment, positioning and irradiance protocols as those used at BM28. Optical (emitting and receiving) fibres (0.6 mm core diameter) (Helma Analytics, Essex, UK) were placed either side of the sample at a 45° incline relative to the sample face and connected to a Nicolet 6700 spectrometer (Thermo Scientific, Warrington, UK). This experimental set up is similar to the schematic shown in **Figure 2**. NIR spectra were collected during photo-polymerisation in transmission mode using a white light source and an InGaAs detector. Spectra were collected in the range of 4000 to 10000 cm^{-1} (4 cm^{-1} spectral resolution) for >360 s with an integration time of 0.1 s. Reactive group conversion was determined from the aliphatic $C{=}CH_2$ IR absorption band (6164 cm^{-1}), located within the methacrylate functional end groups of the Bis-GMA and TEGDMA monomers. The degree of reactive group conversion was calculated using equation (1) as described in section 2.3. Additional

spectral profiles were taken of the empty cell, Mylar windows and of the monomer to correct for background subtraction and intensity normalisation. Data were baseline corrected using Omnic software (Omnic Specta software, version 8.0, Thermo Fisher Scientific, Oxford, UK).

Supporting Data

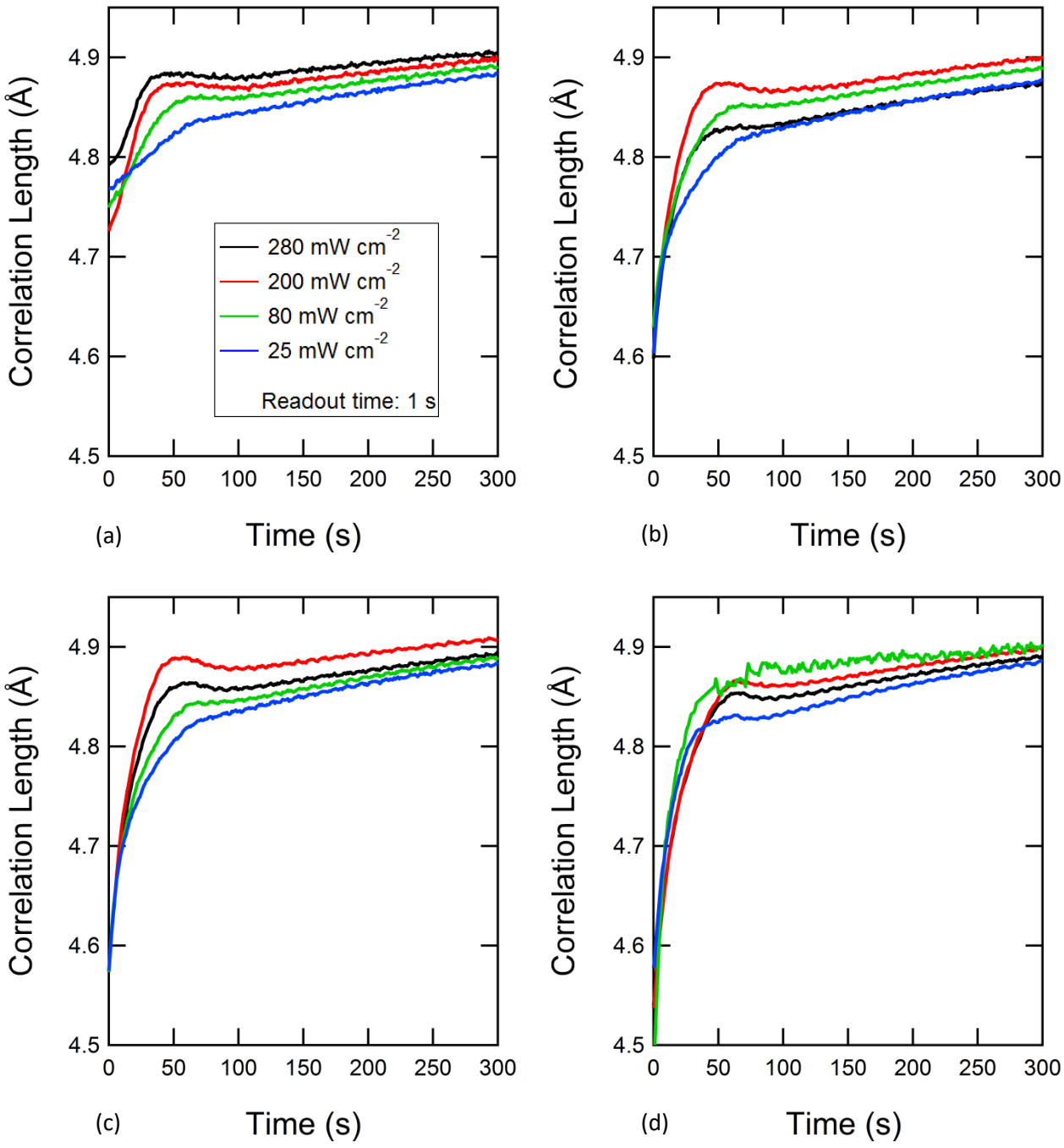

Figure S3. Real time evolution of the correlation length observed in CQ initiated resins for **(a)** 70/30, **(b)** 60/40, **(c)** 50/50 and **(d)** 40/60 wt% blends (Bis-GMA/TEGDMA) during 300 s of photo-polymerisation for a range of reaction rates. All resins display an increase in the correlation length which is larger and faster when a high rate of polymerisation is used. For particularly fast reactions, a subsequent relaxation period can be seen after the initial increase in length, although relaxation is negligible in more fluid blends i.e. Figure S3(c) and (d).

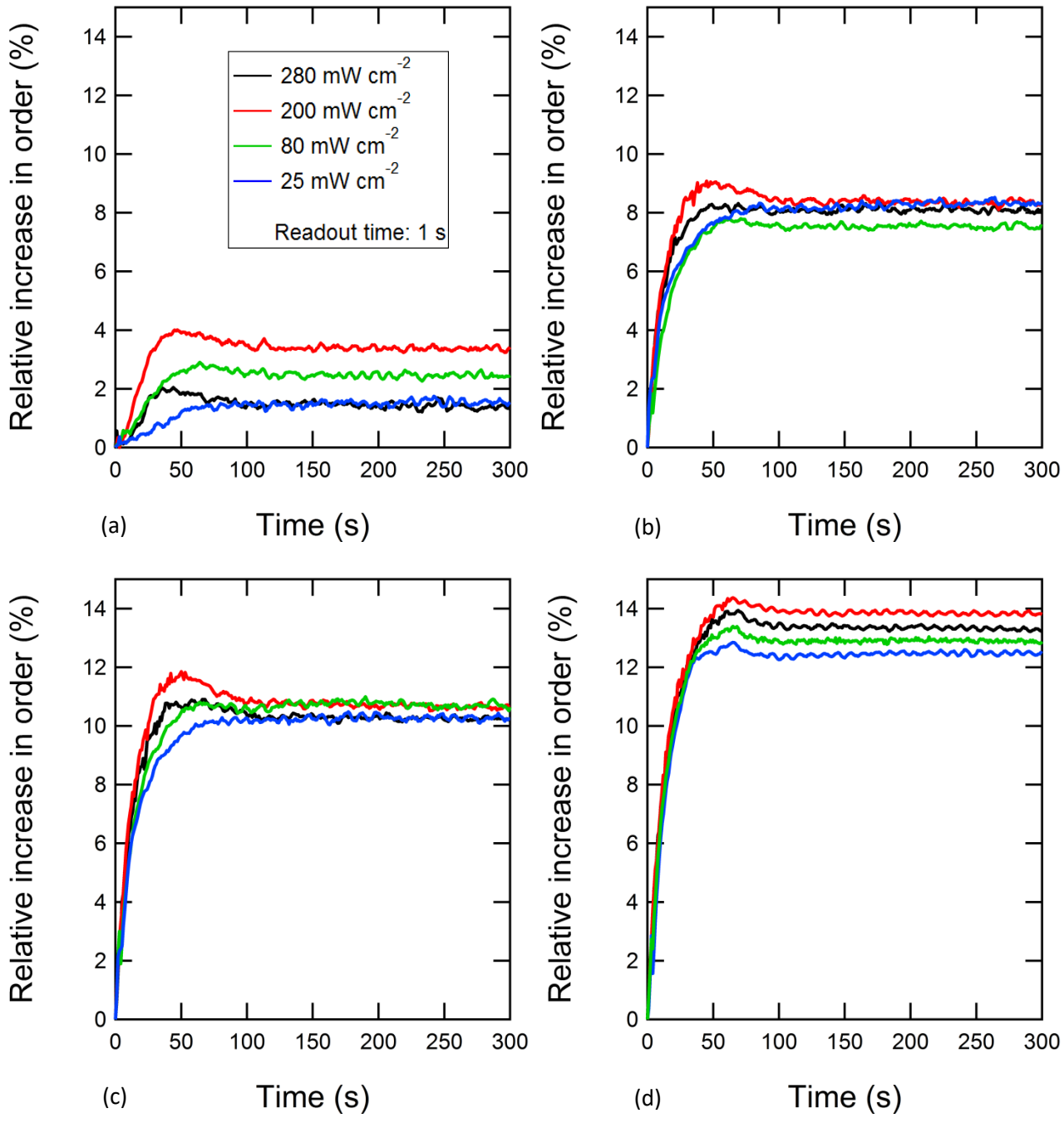

Figure S4. The relative percentage increase in short range structural order during photo-polymerisation as a function of polymerisation rate for resin samples initiated with CQ for **(a)** 70/30, **(b)** 60/40, **(c)** 50/50 and **(d)** 40/60 wt% blends. Changes in structural order are similar and occur simultaneously to those observed in the correlation length for CQ initiated blends.

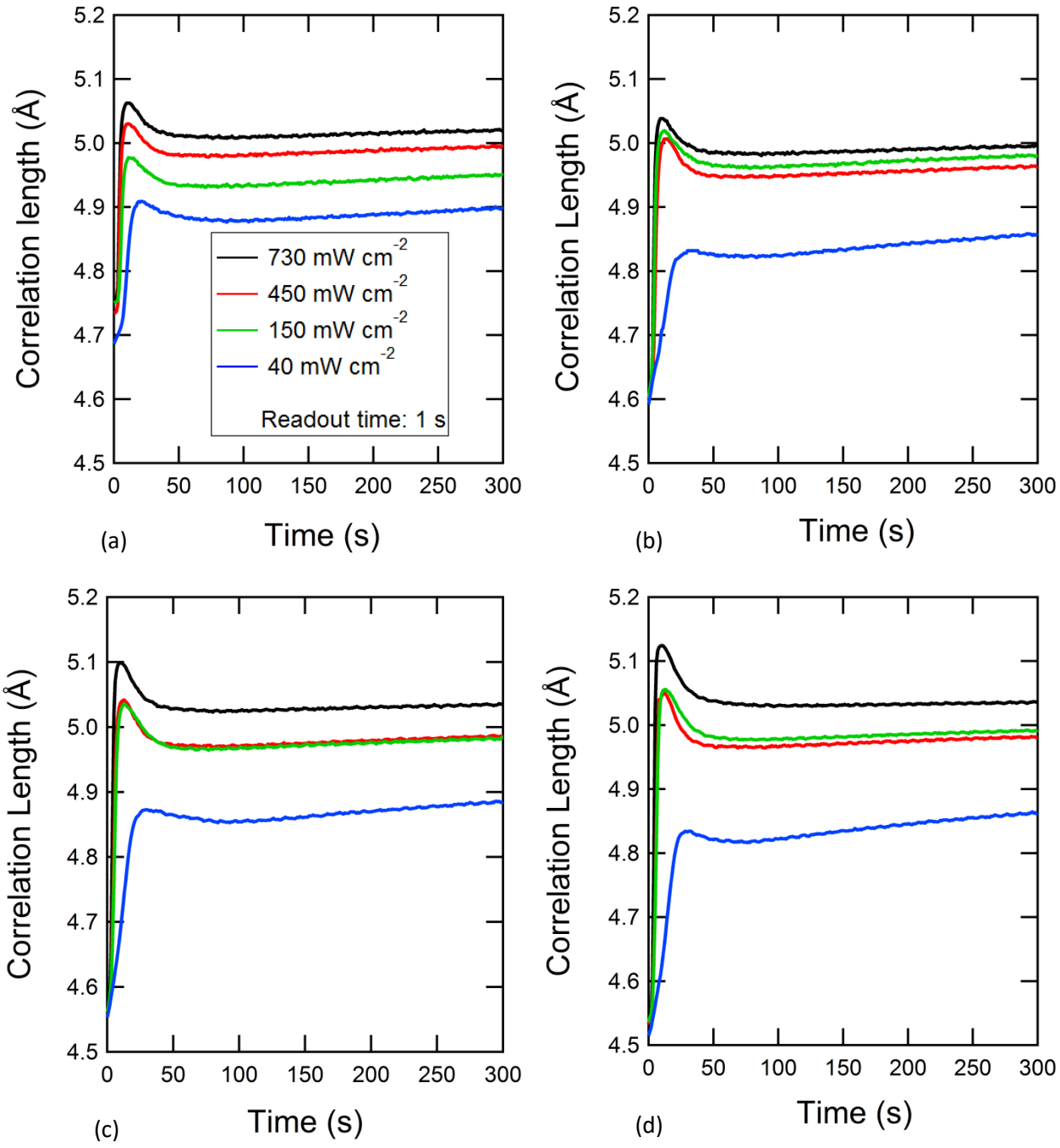

Figure S5. Time resolved changes in the correlation length as observed in TPO initiated resins for **(a)** 70/30, **(b)** 60/40, **(c)** 50/50 and **(d)** 40/60 wt% blends (Bis-GMA/TEGDMA) during 300s of photo-polymerisation for a range of reaction rates. Initial increases in the correlation length upon illumination and subsequent relaxations are larger and more rapid for TPO initiated resins, corresponding to a faster polymerisation rate.

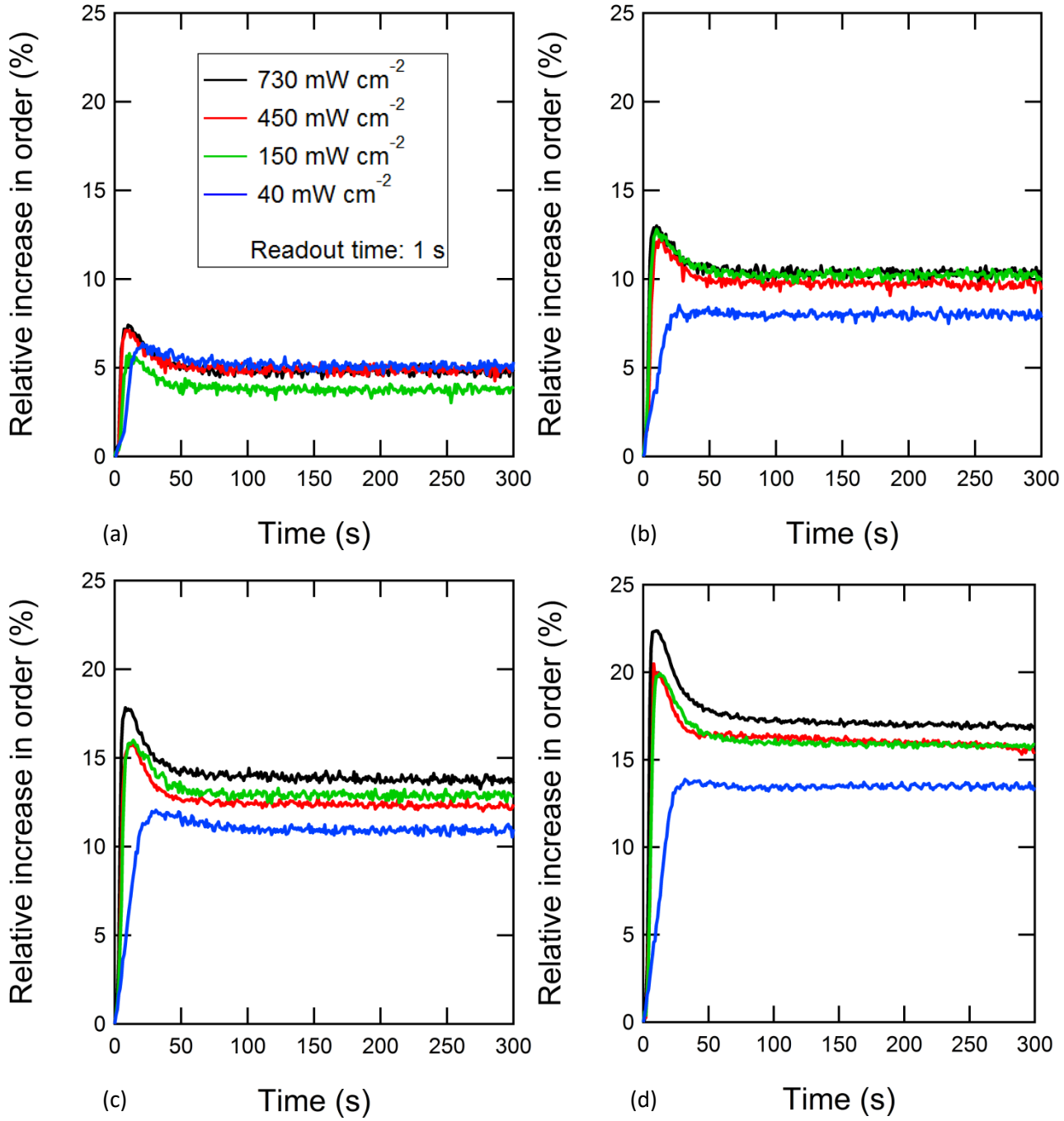

Figure S6. Changes in the relative structural order throughout photo-polymerisation for TPO initiated **(a)** 70/30, **(b)** 60/40, **(c)** 50/50 and **(d)** 40/60 wt% resin blends. Unlike CQ initiated resins, these systems demonstrate a large relaxation.

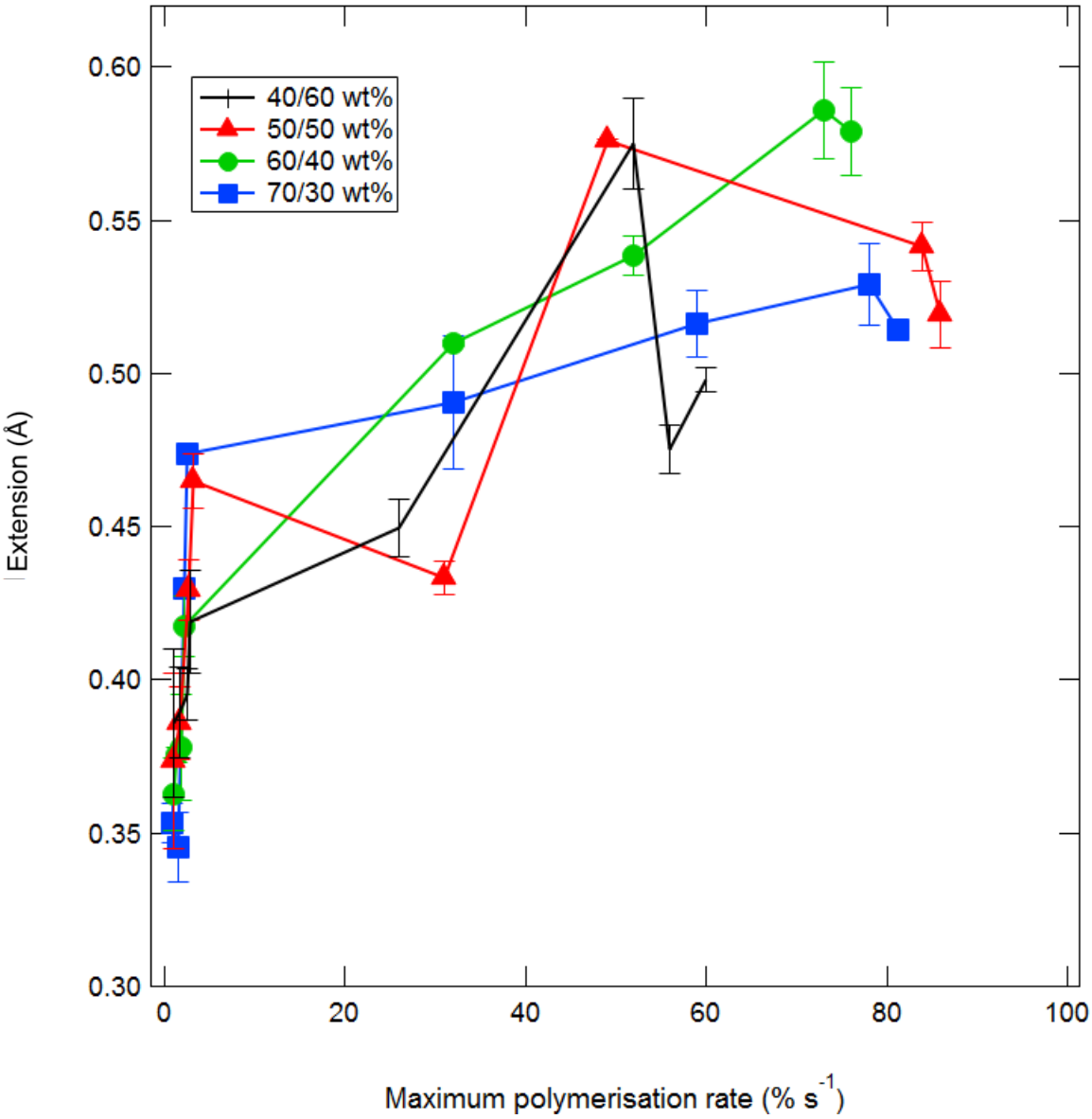

Figure S7. Maximum chain extension for each resin blend (viscosity) normalised to the degree of reactive group conversion, versus polymerisation rate (irradiance). The maximum extension was calculated as the difference between the initial and greatest values of the correlation length for each blend. CQ initiated resins are shown by the first four points and are also inset, whilst the other data points refer to TPO initiated resins.

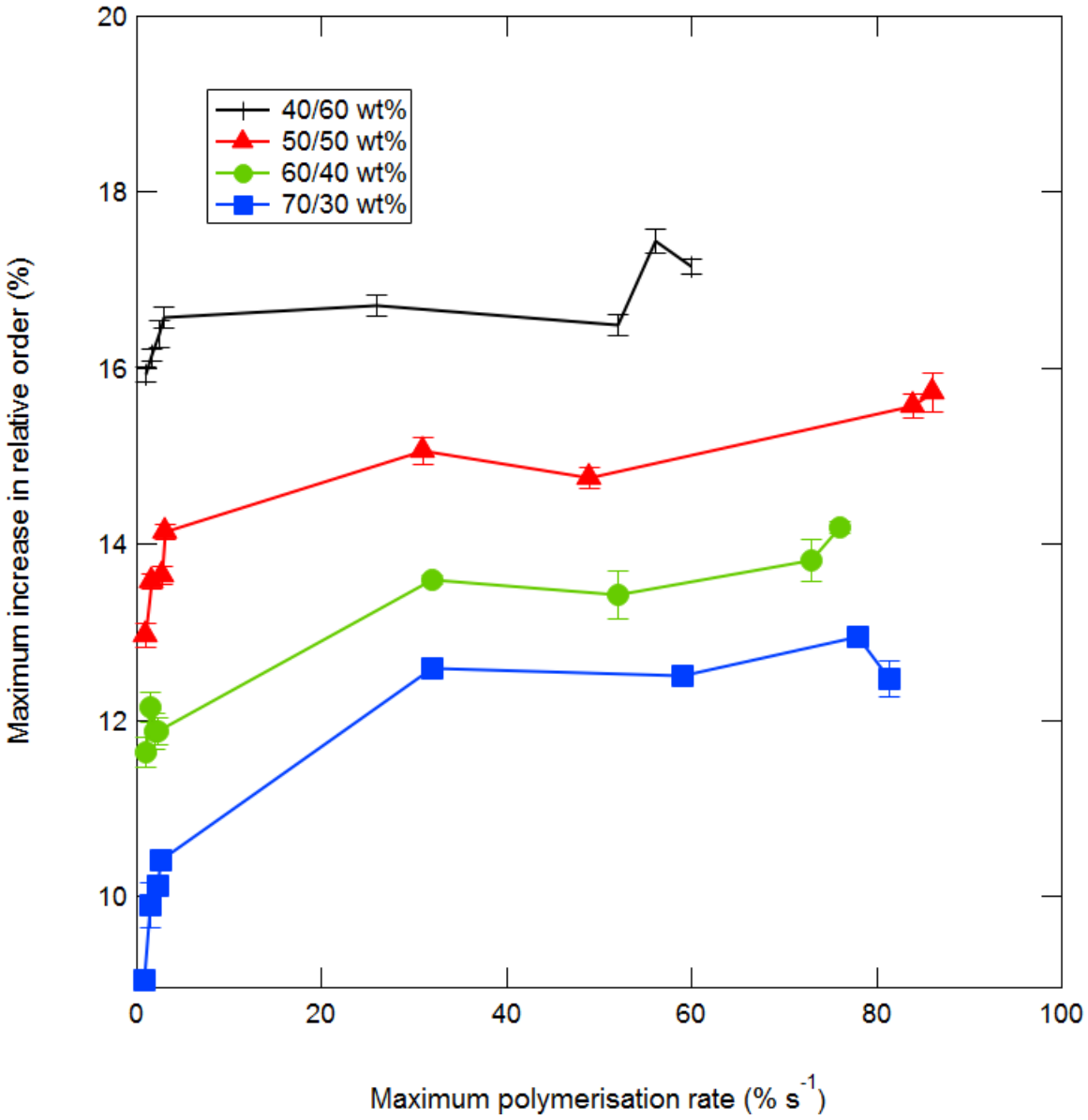

Figure S8. Maximum increase in structural order for each resin blend (viscosity) versus polymerisation rate (irradiance). CQ initiated resins are shown by the first four points, whilst the other data points refer to TPO initiated resins. Error bars represent uncertainty in the values as calculated by propagation of errors. Resins polymerised rapidly demonstrate the greatest increase in structural order, although this is likely an artefact of different conversion values, as a more converted system will inevitably be more ordered.